HHS Public Access

Author manuscript

*Exp Neurol*. Author manuscript; available in PMC 2019 December 01.

Published in final edited form as:

*Exp Neurol*. 2018 December ; 310: 33–47. doi:10.1016/j.expneurol.2018.08.012.

# Transplantation of Human Bone Marrow Stem Cells into Symptomatic ALS Mice Enhanced Structural and Functional Blood-Spinal Cord Barrier Repair

**Svitlana Garbuzova-Davis**[1,2,3,4,*], **Edward Haller**[5], **Stephanie Navarro**[1], **Tony E. Besong**[1], **Kayla J. Boccio**[1], **Surafuale Hailu**[1], **Mohammed Khatib**[1], **Paul R. Sanberg**[1,2,4,6], **Stanley H. Appel**[7], and **Cesario V. Borlongan**[1,2]

[1]Center of Excellence for Aging & Brain Repair, University of South Florida, Morsani College of Medicine, Tampa, Florida 33612, United States of America

[2]Department of Neurosurgery and Brain Repair, University of South Florida, Morsani College of Medicine, Tampa, Florida 33612, United States of America

[3]Department of Molecular Pharmacology and Physiology, University of South Florida, Morsani College of Medicine, Tampa, Florida 33612, United States of America

[4]Department of Pathology and Cell Biology, University of South Florida, Morsani College of Medicine, Tampa, Florida 33612, United States of America

[5]Department of Integrative Biology, University of South Florida, Tampa, Florida 33620, United States of America

[6]Department of Psychiatry, University of South Florida, Morsani College of Medicine, Tampa, Florida 33612, United States of America

[7]Stanley H. Appel Department of Neurology, Houston Methodist Neurological Institute, Houston, Texas 77030, United States of America

## Abstract

Accumulating evidence shows alterations in the blood-brain barrier (BBB) and blood-spinal cord barrier (BSCB) in ALS patients and in animal models of disease, mainly by endothelial cell (EC) damage. Repair of the altered barrier in the CNS by replacement of ECs via cell transplantation may be a new therapeutic approach for ALS. Recently, we demonstrated positive effects towards BSCB repair by intravenous administration of unmodified human bone marrow CD34+ (hBM34+) cells at different doses into symptomatic ALS mice. However, particular benefits of these transplanted cells on microvascular integrity in symptomatic ALS mice are still unclear. The aim

[*]Author for correspondence: Svitlana Garbuzova-Davis, Ph.D., D.Sc., Center of Excellence for Aging and Brain Repair, Department of Neurosurgery and Brain Repair, University of South Florida, Morsani College of Medicine, 12901 Bruce B. Downs Blvd., MDC 78, Tampa, FL 33612, United States of America, Tel: 813-974-3189, Fax: 813-974-3078, sgarbuzo@health.usf.edu.

Declaration of conflicting interest

The authors declare that they have no conflict of interest.

of the present study was to determine the structural and functional spinal cord capillary integrity in symptomatic ALS mice after intravenous administration of hBM34+ cells. The G93A mice at 13 weeks of age intravenously received one of three different cell doses ($5\times10^4$, $5\times10^5$, or $1\times10^6$) and were euthanized at 17 weeks of age (4 weeks post-transplant). Control groups were media-treated and non-carrier mutant SOD1 gene mice. Capillary ultrastructural (electron microscopy), immunohistochemical (laminin and HuNu), and histological (myelin and capillary density) analyses were performed in the cervical and lumbar spinal cords. Capillary permeability in the spinal cords was determined by Evans Blue (EB) injection. Results showed significant restoration of ultrastructural capillary morphology, improvement of basement membrane integrity, enhancement of axonal myelin coherence, and stabilization of capillary density in the spinal cords primarily of ALS mice receiving the high dose of $1\times10^6$ cells. Moreover, substantial reduction of parenchymal EB levels was determined in these mice, confirming our previous results on capillary permeability.

Additionally, transplanted cells were detected in blood smears of sacrificed late symptomatic mice by HuNu marker. Altogether, these results provide *novel* evidence that unmodified bone marrow hematopoietic stem cell treatment at optimal dose might be beneficial for structural and functional repair of the damaged BSCB in advanced stage of ALS potentially resulting in delayed disease progression by increased motor neuron survival.

**Keywords**

ALS; G93A SOD1 mice; blood-spinal cord barrier; human bone marrow CD34+ cells; transplantation; repair

## 1. Introduction

Amyotrophic lateral sclerosis (ALS) is a fatal disease characterized by motor neuron degeneration in the brain and spinal cord. The disease progresses gradually from initial muscle weakness of legs or arms to muscle atrophy leading to paralysis and death of the patient mainly due to respiratory failure. Mortality usually occurs within 3 to 5 years from appearance of first symptoms (Calvo et al., 2014; Gordon, 2011; Kiernan et al., 2011; Sorarù et al., 2010; Talbot, 2009; Wijesekera and Leigh, 2009). About 50% of patients die within 30 months of disease symptom onset; 20% of patients survive 5 years, and up to 10% live more than 10 years after symptom onset. ALS cases are classified as either sporadic (SALS, 90–95% cases, idiopathic) or familial (FALS, 5–10% cases, a genetic link), with both forms sharing similar clinical presentation and underlying pathology. The treatment options for ALS patients are limited and mainly supportive. The only FDA approved drugs for ALS are riluzole (Hugon, 1996; Miller et al., 2003) and the recently approved edaravone (Radicava) (Rothstein, 2017).

From the initial description of ALS as a rapidly progressive neuromuscular disorder by French neurologist Jean-Martin Charcot in 1869 (Kumar et al., 2011), clinical and scientific efforts to understand ALS pathogenesis have grown extensively emphasizing the complexity of intrinsic and extrinsic factors underlying this disease. Numerous hypotheses regarding causes or contributors to the death of motor neurons in ALS have been proposed (Cleveland

and Rothstein, 2001; Cui et al., 2014; D'Amico et al., 2013; Kolind et al., 2013; Martin et al., 2000; McCombe and Henderson, 2011; Niebroj-Dobosz et al., 2007; Nonneman et al., 2014; Papadimitriou et al., 2010; Pratt et al., 2012; Prell et al., 2015; Rodrigues et al., 2014, 2012; Rothstein, 2009; Strong et al., 2005; Zhao et al., 2013). Although multiple pathogenic effectors (glutamate excitotoxicity, oxidative stress, protein aggregation, glial cell dysfunction, myelin disruption, immune/inflammatory reactivity, etc.) are known contributors to the diffuse motor neuron degeneration in ALS, relatively recent evidence of vascular pathology has newly identified ALS as a neurovascular disease (Garbuzova-Davis et al., 2011).

Our original studies (Garbuzova-Davis et al., 2007a, 2007b) showing impairment of the blood-CNS barrier (B-CNS-B) in symptomatic ALS mice have spurred various investigations demonstrating that this barrier damage likely represents an additional pathogenic disease mechanism. Convincing results showed structural and functional alterations in the blood-brain barrier (BBB) and blood-spinal cord barrier (BSCB) in ALS patients (Garbuzova-Davis et al., 2012a; Henkel et al., 2009; Winkler et al., 2013) and in animal models of disease (Bataveljic et al., 2012, 2009; Miyazaki et al., 2011; Nicaise et al., 2009; Zhong et al., 2008).

Degeneration of endothelial cells (ECs) and astrocyte end-feet processes surrounding microvessels, impairment of endothelial transport system, damaged mitochondria in EC and neuropil, and dysfunction of tight junction proteins are all likely primary effectors compromising BBB/BSCB integrity. Moreover, microvascular leakage and rupture, perivascular edema, decreased capillary length and blood flow have been shown in the spinal cords of ALS mice. Also, substantial loss of axonal myelinization was observed in the brainstem, cervical and lumbar spinal cords of ALS mice, mainly at late stage of disease (Garbuzova-Davis et al., 2007a). Based on these evidences, molecular biomarkers of transmembrane proteins such as water (aquaporin-4, AQP4) and potassium (Kir4.1) channels have been proposed for BBB/BSCB maintenance in ALS (reviewed in (Bataveljic et al., 2014)). Thus, the dysfunctional B-CNS-B may be an essential contributor to ALS pathogenesis, permitting entry of numerous detrimental factors from the systemic circulation to the CNS and accelerating motor neuron degeneration (Garbuzova-Davis et al., 2008b).

Although specific B-CNS-B alterations have been noted in ALS patients versus an animal model of disease (Garbuzova-Davis and Sanberg, 2014), the damaged capillary endothelium is a shared pathology in patients and an animal model of ALS. We hypothesized that repair of the altered B-CNS-B by replacement of endothelial cells via cell administration may be a new therapeutic approach for this disease. Recently, we demonstrated (Garbuzova-Davis et al., 2017) that intravenous administration of human bone marrow CD34+ (hBM34+) cells at different doses into symptomatic ALS mice delayed disease progression, maintained motor neuron survival, reduced macro- and microgliosis, preserved perivascular end-feet of astrocytes, and decreased capillary permeability in the spinal cord. Importantly, transplanted cells differentiated into endothelial cells and engrafted within spinal cord capillaries. Moreover, our most recent study (Eve et al., 2018) showed a significant decrease of microhemorrhages in the spinal cords of ALS mice treated with hBM34+ cells. These effects

were mostly determined in mice receiving the high cell dose and might represent processes towards BSCB repair.

However, the particular beneficial effects of administered hBM34+ cells on microvascular integrity in symptomatic ALS mice still need clarification.

The aim of this study was to determine the structural and functional capillary status in the spinal cord of symptomatic ALS mice after intravenous administration of hBM34+ cells at different doses. First, the ultrastructure of microvessels was analyzed in spinal cord areas of anterior motor neurons. Second, the efficacy of cell treatment on capillary permeability was evaluated. Finally, morphological axon/myelin coherence and capillary density were examined in the spinal cords. These study results provide important evidence for establishment of BSCB reparative processes in ALS via stem cell therapy.

## 2. Materials and methods

### 2.1. Ethics Statement

All described procedures were approved by the Institutional Animal Care and Use Committee at USF and conducted in compliance with the *Guide for the Care and Use of Laboratory Animals*. All mice were housed in a temperature-controlled room (23°C) and maintained on a 12:12 h dark: light cycle (lights on at 06:00 AM). Food and water were available *ad libitum*. Upon progression of neurological symptoms, a highly palatable liquid nutritional supplement was placed on the cage floor, ensuring access by the animal.

### 2.2. Animals

All animals used in the study were obtained from The Jackson Laboratory, Bar Harbor, ME, USA. Seventy-four transgenic male B6SJL-Tg(SOD1*G93A)1Gur/J mice, over-expressing human SOD1 carrying the Gly93→Ala mutation (G93A SOD1) at 7 weeks of age, were randomly assigned to one of four groups receiving different doses of $hBM34^+$ cells or media: *Group 1* - hBM34+ ($5\times10^4$ cells/mouse, low dose, n=15), *Group 2* - hBM34+ ($5\times10^5$ cells/mouse, mid dose, n=16), *Group 3* - hBM34+ ($1\times10^6$ cells/mouse, high dose, n=23), and *Group 4*- Media (n=20). At 8 weeks of age and then weekly, mouse body weight was monitored as an indicator of health. Initially,G93A mice demonstrate disease symptoms such as hindlimb tremor and then reductions in body weight and/or extension reflex appear at 12–13 weeks of age (Garbuzova-Davis et al., 2017), considered as early symptomatic disease stage. At 13 weeks of age, ALS mice intravenously (iv, jugular vein) received either the appropriate $hBM34^+$ cell dose or an equal volume of media. A non-transplant control group (*Group 5)*, consisted of mice from the background strain that did not carry the mutant SOD1 gene (control, n=16). At 14 weeks of age and weekly until 17 weeks of age, mice were again observed for symptoms of disease progression.

### 2.3. Cell preparation and transplant procedure

Cryopreserved human bone marrow CD34+ cells ($hBM34^+$) were purchased from AllCells (Alameda, CA, USA). According to the company report, cells were obtained from healthy donors and tested negative for viral (HIV, HBV, and HCV) screening and microbial growth.

Also, the commercial cell analysis report provided information regarding viability (~95%) and purity (~98%) of hBM34$^+$ cells via FACS of CD34-FITC. Preparation of hBM34$^+$ cells for transplantation was previously described in our recent publication (Garbuzova-Davis et al., 2017). Briefly, hBM34$^+$ cells were thawed rapidly at 37°C and then transferred slowly with a pipette into a centrifuge tube containing 10 ml of Dulbecco's Phosphate Buffered Saline 1X (DPBS), pH 7.4 (Mediatech, Inc., Manassas, VA, USA). The cells were centrifuged (200 g/10 min) at room temperature (RT), the supernatant discarded and the process repeated. After the final wash, cell viability was assessed using the 0.4% trypan blue dye exclusion method before and after transplantation. Transplant cell concentrations were adjusted for each group: 250 cells/μl ($5\times10^4$ cells/200 μl/injection, Group 1), 2,500 cells/μl ($5\times10^5$ cells/200 μl/injection, Group 2), and 5,000 cells/μl ($1\times10^6$ cells/200 μl/injection, Group 3).

The hBM34+ cells were delivered intravenously via the jugular vein of mice under anesthesia with isofluorane (2–5% at 2L $O_2$/min) as we previously described (Garbuzova-Davis et al., 2008a, 2003) with minor modifications (Garbuzova-Davis et al., 2017). Briefly, a 26-gauge needle was inserted into the jugular vein of anesthetized animals and a solution containing the cells was injected during 3 min. After transplantation, the incision was closed and sutured using a stainless steel wound clip. The Media mice in Group 4 received 200 μl of DPBS, the same volume administered to the cell-transplanted mice. Animals in Groups 1–4 received cyclosporine A (CsA, 10 mg/kg ip) daily for the entire post-transplant period.

### 2.4. Perfusion and tissue preparation

All cell-treated, media-treated, and control mice were sacrificed under Euthasol® (0.22 ml/kg body weight) and perfused transcardially with 0.1 M phosphate buffer (PB, pH 7.2) followed by 4% paraformaldehyde (PFA) in PB solution under pressure control fluid delivery at 80–85 mm Hg to avoid capillary rupture at 17 weeks of age (corresponding to 4 weeks after initial treatment at symptomatic disease stage) for ultrastructural (electron microscopy), immunohistochemical, and histological analyses in the cervical and lumbar spinal cords. Mouse age of 17 weeks for sacrifice was the same age as we reported earlier (GarbuzovaDavis et al., 2017) and considered near end-stage of disease. Since our previous report (Garbuzova-Davis et al., 2017) showed that a high hBM34+ cell dose ($1 \times 10^6$) administered into symptomatic ALS mice significantly decreased capillary permeability in the spinal cords, the current study was extended to determine capillary leakage in the spinal cords of mice receiving low and mid cell doses. The mice (Group 1: n=8; Group 2: n=9; Group 3: n=9; Group 4: n=10) and controls (Group 5; n=10) were injected with 2% Evans Blue dye (EB, Sigma-Aldrich, St. Louis, MO, USA) in saline solution (4 ml/kg body weight) via the tail vein at 30 min prior to perfusion as described (Garbuzova-Davis et al., 2017). Prior to perfusion, blood samples (about 500–700 μl) were taken through cardiac puncture from randomly selected cell-treated, media-treated, and control mice (n=56/group) and collected into serum separation tubes (Corvac™) for 10 minutes at RT. Sera were obtained after centrifugation at 1200 rpm for 15 minutes. Mice assayed for EB extravasation received only the PB solution. After perfusion, the entire spinal cords were rapidly removed from cell-treated (n=5–6/group), media-treated (n=6) and controls (n=7) for the EB extravasation assay described below. In remaining mice (n=3–4/group) receiving EB

injection, the cervical and lumbar spinal cord segments were removed, post-fixed intact in 4% PFA for 24–48 hours, and then cryoprotected in 20% sucrose in 0.1 M PB overnight. Coronal spinal cord tissues were cut at 30 μm in a cryostat, every fifth section was thaw-mounted onto slides, and the tissue was stored at 20°C for immunohistochemical analyses of capillary EB leakage. Also, mice (n=3–4/group) were perfused and their spinal cords were removed, post-fixed, cryoprotected, and cut as described above for immunohistochemical analyses of capillary laminin expression. Additionally, blood was collected during perfusion of ALS mice (n=8) only receiving high hBM34+ cell dose ($1 \times 10^6$) and media-treated mice (n=3). Blood smears were obtained and then fixed in methanol for 10 min for later immunocytochemical analyses of transplanted cells.

Mice assayed for electron microscope analysis were randomly chosen from cell-treated, media-treated, and control groups (n=3/group). Mouse cervical and lumbar spinal cords were immediately removed after perfusion with 4% PFA in 0.1 M PB and fixed in the same fixative for 16–24 hours at 4°C. The next day, spinal cords were coded and cut into 1 mm slices. Tissues were then fixed overnight in 2.5% glutaraldehyde in 0.1M PB (Electron Microscopy Sciences, Inc., Hatfield, PA) at 4°C and stored for later electron microscope processing.

### 2.5. Electron microscopy

Since compromised B-CNS-B integrity was determined in motor neuron areas in ALS mice at early and late disease stages (Garbuzova-Davis et al., 2007a, 2007b), structural analyses of cervical and lumbar spinal cord microvessels were performed using electron microscopy. Briefly, spinal cord tissue samples were postfixed in 1% osmium tetroxide (Electron Microscopy Sciences, Inc., Hatfield, PA) in 0.1M PB for 1 hour at RT and then dehydrated in a graded series of acetone dilutions. Tissues were transferred to a 50:50 mix of acetone and LX112 epoxy resin embedding mix (Ladd Research Industries, Burlington, VT) and infiltrated with the mix for 1 hour. The tissues were then transferred to a 100% L×112 embedding mix and infiltrated with fresh changes of this embedding mix. The tissues were further infiltrated overnight in fresh embedding medium at 4ºC. On the following day, the tissues were embedded in a fresh change of resin in tissue capsules. The blocks were polymerized at 70°C in an oven overnight. The blocks were trimmed and then sectioned with a diamond knife on a Leica Ultracut ultramicrotome. Thin sections were cut at 80–90 nm, placed on copper grids, and stained with uranyl acetate and lead citrate.

### 2.6. BSCB integrity analysis

For analysis of BSCB ultrastructure, microvessels in the cervical and lumbar spinal cords of cell-treated, media-treated, and controls were examined by an investigator blinded to the animal groups, using coded sections, and photographed with an AMT ActiveVu XR 16 digital camera, (Advanced Microscopy Techniques, Woburn, MA) attached to a FEI Morgagni transmission electron microscope (FEI, Inc., Hillsboro, OR), at 60kV.

Analyses of capillary morphologies in the spinal cords of cell-treated, media-treated, and controls were performed based on electron microscopic (EM) images. Total analyzed capillaries were: *the cervical spinal cord* – control (n=54), media (n=78), low dose (n=121),

mid dose (n=99), and high dose (n=109); *the lumbar spinal cord* – control (n=55), media (n=72), low dose (n=127), mid dose (n=89), and high dose (n=81). Capillaries were considered of *normal morphology* if a) endothelial cells (ECs) were intact and the basement membrane was a single layer surrounded by astrocytes or oligodendrocytes, b) mitochondria had well preserved cristae in the cytoplasm of all cells including ECs, c) normal neuropil surrounded the capillaries, and d) no evidence of intra- or extracellular edema was displayed. *Moderately impaired* capillary morphology was determined by appearance of a) EC cytoplasm with some vacuoles and dilated endoplasmic reticulum, b) swollen mitochondria in ECs and in the neuropil, and/or c) minor extracellular edema between areas of neuropil and near capillaries. *Severely compromised* capillary morphology was determined by the presence of a) substantially vacuolated ECs, b) necrotic ECs with condensed cytoplasm, c) ECs detached from basement membrane, d) vacuolated mitochondria in the cytoplasm of ECs and neuropil with swelling and disruption of cristae, e) degenerated astrocyte end-feet surrounding the capillaries with free floating swollen mitochondria, and/or f) extensive protein-filled extracellular edema around the capillaries. Quantitative analysis for each capillary category was presented as a percentage of total capillary numbers per animal group for both cervical and lumbar spinal cords.

### 2.7. BSCB permeability

Evans Blue (EB) dye, 961 Da, was used as a tracer for assessing BSCB disruption. The EB extravasation assay was performed as previously described (Garbuzova-Davis et al., 2017, 2016, 2014, 2007b). Briefly, after perfusion, mouse spinal cords were weighed and placed in 50% trichloroacetic acid solution (Sigma). Following homogenization and centrifugation, the supernatant was diluted with ethanol (1:3) and loaded into a 96 wellplate in triplicate. Sera were diluted with ethanol (1:10,000) and loaded separately into a 96-well plate in triplicate also. The dye was measured with a spectrofluorometer (Gemini EM Microplate Spectrofluorometer, Molecular Devices) at excitation of 620 nm and emission of 680 nm (Ay et al., 2008; Garbuzova-Davis et al., 2017). Calculations were based on external standards in the same solvent. The EB content in tissue was quantified from a linear standard curve derived from known amounts of the dye and was normalized to tissue weight (μg/g). For sera, EB concentration was quantified similarly and presented as μg/mL. All measurements were performed by two experimenters blinded to the experiment.

### 2.8. Immunohistochemical staining

For identification of vascular EB leakage, serial spinal cord tissue sections from EB injected mice (n=3–4/group) were thaw-mounted on slides and then rinsed several times in PBS to remove the freezing medium. The slides were coverslipped with Vectashield® containing DAPI (Vector Laboratories, USA) and examined under epifluorescence using an Olympus B×60 microscope.

In a separate set of cervical and lumbar spinal tissue sections from randomly selected mice (n=34/group), immunohistochemical staining of the basement membrane protein (laminin) was performed as previously described (Garbuzova-Davis et al., 2007b). Briefly, spinal cord tissues were pre-incubated with 10% goat serum and 0.3% Triton × 100 in PBS for 60 min at RT and then stained with rabbit anti-laminin polyclonal antibody (1:200, Cat. No. ab11575,

Abcam, USA) overnight at 4°C. The next day, the slides were incubated with goat anti-rabbit secondary antibody conjugated to rhodamine (1:1000, Cat. No. A11012, Invitrogen, USA) for 2 hours. After several rinses in PBS, slides were coverslipped with Vectashield® containing DAPI (Vector Laboratories, USA) and examined under epifluorescence using an Olympus BX60 microscope. Analyses of laminin immunoexpression in the cervical and lumbar spinal cords of cell-treated, media-treated, and control mice were performed in the ventral horns by an investigator blinded to the experiments. Immunohistochemical image analysis for laminin was performed by measuring intensity of fluorescent expression (%/$mm^2$) in NIH ImageJ (version 1.46) software. Thresholds for detection of laminin fluorescent expressions were adjusted for each image to eliminate background noise as previously described (Garbuzova-Davis et al., 2017). Immunohistochemical images (n=10 images/spinal cord segment) were taken in randomly selected areas from right and left ventral gray matter of the cervical and lumbar spinal cords at 10×. Fluorescent intensity (%/$mm^2$) was measured in the entire image. Data are presented as averages of laminin immunoexpression from both sides.

For identification of intravenously transplanted hBM34+ cells within blood circulation, blood was collected during perfusion of ALS mice (n=8) receiving high hBM34+ cell dose ($1 \times 10^6$) and media-treated mice (n=3) only. Blood smears were obtained and fixed in methanol for 10 minutes. Also, hBM34+ cell smears served as positive controls. Immunofluorescent staining with the human-specific nuclei marker (HuNu) was performed as we described previously (Garbuzova-Davis et al., 2017, 2012b, 2008b). Briefly, the mouse monoclonal antibody (HuNu, 1:100, Cat. No. 1281, Millipore Sigma, USA) was combined with the secondary antibody, monovalent goat anti-mouse Fab' fragment conjugated to rhodamine (1:200; Cat. No. 115–607-003, Jackson ImmunoResearch, USA), and incubated at RT for 2 hours. The blood and cell smears were preincubated with 1% normal human serum (NHS) and 0.5% Triton X 100 in PBS for 30 min at RT and subsequently incubated with the previously prepared antibody cocktail overnight at 4°C. Next day, slides were thoroughly washed in PBS and coverslipped with Vectashield® containing DAPI (Vector Laboratories, USA). The slides were then examined under epifluorescence using an Olympus BX60 microscope. Cells immunopositive for HuNu were counted manually from the entire slide at 40X and determined as a percentage of total nucleated cells for each mouse.

To test for specificity of the immunostaining for laminin and HuNu, the primary antibodies were omitted from control slides. No staining was observed in the control sections.

### 2.9. Histological staining and analysis

As part of preparing the spinal cord tissues for EM, tissue post-fixation in 2.5% glutaraldehyde, osmication in 1% osmium tetroxide, acetone dehydration, and embedding in LX112 epoxy resin were performed as described above. Tissues were embedded in plastic blocks and semi-thin tissue sections (0.35 μm) were cut using a Leica Ultracut ultramicrotome and then mounted on glass slides. Spinal cord sections were stained with 1% toluidine blue (Fisher Scientific, USA) for 1 minute, rinsed in water, de-stained in 95% ethanol, dried, and then coverslipped. This specific tissue preservation and fixation result in

conventional toluidine blue-stained myelinated fibers in the spinal cords (Di Scipio et al., 2008; Feirabend et al., 1998). Morphological analyses of axonal myelin sheaths were performed in the lumbar spinal cords at L3-L4 segments of cell-treated, media-treated, and controls (n=3/group). The phase contrast images were taken at 4X using an Olympus B × 60 microscope. Histological image analysis for myelin was performed by measuring intensity of staining expression (%/mm$^2$) in NIH ImageJ (version 1.46) software. Thresholds for detection of myelin staining were adjusted for each image to eliminate background noise as previously described (Garbuzova-Davis et al., 2017). Images (n=2–3 images/spinal cord side/group) were taken in selected areas from lateral funiculus (LF) and ventral horn (VH) on both sides of the lumbar spinal cords at 10×. Myelin intensity (%/mm$^2$) was measured in the entire image. Additionally, capillary numbers were counted at 3–10 μm in diameter on both sides of lumbar VH images (n=3/side/group) at 40X using NIH ImageJ software. Capillary density (number/mm$^2$) was determined for each entire image. Data are presented as averages of capillary density in VH of each spinal cord side.

### 2.10. Statistical analysis

Data are presented as means ± S.E.M. One-way ANOVA with post-hoc Tukey HSD (Honesty Significant Difference) multiple comparison test using online statistical software (astatsa.com, 2016 Navendu Vasavada) was performed for statistical analysis. Significance was defined as $p < 0.05$.

## 3. Results

### 3.1. Ultrastructural characteristics of capillaries in the spinal cord

Ultrastructure of microvasculature in the cervical and lumbar spinal cords of cell-treated, media-treated, and controls at 17 weeks of age was analyzed using an electron microscope (EM). In ALS mice, EM analysis was conducted 4 weeks after cell transplantations or media-injections to reveal structural BSCB status.

Examination of the immersion-fixed tissues from all animals showed well-preserved and well-processed tissues.

**3.1.1. Cervical spinal cord—**Ultrastructural examination of the cervical spinal cord from control mice demonstrated the normal appearance of capillaries and perivascular astrocytes (**Figure 1Aa**). All capillaries consisted of a single layer of endothelial cells (ECs), forming a lumen, and pericytes. The basement membrane was surrounded by astrocyte foot processes. Myelinated axons showed typical morphology in neuropil. Mitochondria displayed a normal pattern of cristae. Significant ultrastructural abnormalities were observed in the ventral spinal horn in mediatreated ALS mice (**Figure 1Ab**). Swollen ECs with cytoplasmic vacuolization or large autophagosomes were determined in numerous capillaries. Free floating mitochondria, some of them swollen, were seen in the remains of perivascular astrocyte processes. Extensive protein-filled extracellular edema was found around capillaries. Myelin surrounding axons appeared degenerated. There was no substantial capillary morphological improvement in ALS mice receiving the low hBM34+ cell dose (**Figure 1Ac**). Swollen ECs, degenerated astrocyte end-feet, and perivascular

edema were noted. Moderate enhancement of capillary ultrastructure by reduction of perivascular edema and near normal EC appearance was determined in some microvessels of ALS mice with the mid cell dose (**Figure 1Ad**). However, some axons with reduced myelin sheathing were evident. In ALS mice receiving the high hBM34+ cell dose, numerous capillaries demonstrated typical ultrastructural morphology of ECs and pericytes (**Figure 1Ae and Af**). Nevertheless, some areas of perivascular edema between capillary and astrocyte end-feet and degenerated myelinated axons were found. Capillary tight junctions, however, were well defined.

Quantitative analysis of capillary morphology in the cervical spinal cords demonstrated a higher percentage of capillaries with normal morphology (70.63 ± 1.52%) vs. moderate impairment (29.37 ± 1.52%) in control mice at 17 weeks of age (**Figure 1B**). No severely damaged capillaries were determined in control mice. Media-injected ALS mice at same age showed a significant ($p = 0.001$) reduction of morphologically normal capillaries (22.40 ± 6.83%) and an increase in capillaries with moderate impairment (43.37 ± 6.78%) compared to controls. A high percentage of severely impaired capillaries (34.23 ± 4.31%) was determined in media mice (**Figure 1B**). The percentage of capillaries with normal morphology gradually increased in cell-treated vs. media ALS mice with cell dosage: low dose - 17.63 ± 1.87%, mid dose - 33.40 ± 4.48%, and high dose - 45.63 ± 9.35% ($p = 0.033$). Of note, there was a significant ($p = 0.011$) increase of normal capillaries in mice receiving the high cell dose vs. the low cell dose treatment. At the same time, the percentage of severely damaged microvessels decreased with dosage: low dose - 31.63 ± 3.62%, mid dose - 18.87 ± 2.70% ($p = 0.038$), and high dose - 17.27 ± 4.75% ($p = 0.024$) (**Figure 1B**). However, increase of capillaries with moderate morphological impairment was noted only in low dose - 50.73 ± 1.86% and mid dose - 47.73 ± 4.90% vs. media mice. Mice receiving the high cell-dose showed a slight non-significant decrease of these moderately impaired capillaries (37.13 ± 5.78%) compared to media-treated animals (**Figure 1B**).

**3.1.2. Lumbar spinal cord—**Similarly to the cervical spinal cords, capillaries in the ventral horn of the lumbar spinal cords from control mice appeared morphologically intact and were composed of a single layer of EC, pericytes, basement membrane, tight junction, and adjacent astrocyte end-feet (**Figure 2Aa**). Myelin surrounding axons and mitochondria in neuropil were well preserved. Media-treated ALS mice showed degenerated ECs within capillary lumen and protein-filled extracellular edema around capillaries (**Figure 2Ab**). Swollen mitochondria were also observed in the neuropil and within axons. There was evidence of myelin disruption in surrounding axons. In mice receiving the low or mid cell dose treatment, improvement of capillary morphology was not indicated. Swollen or vacuolated ECs in major capillaries was detected in low-cell (**Figure 2Ac**) and mid-cell (**Figure 2Ad**) dose treated mice. Also, significant extracellular edema was determined in these cell-treated mice. Free floating mitochondria in space of degenerated astrocyte end-feet were observed. Mitochondria with disrupted cristae were seen in axon (top left, **Figure 2Ad**) in addition to degenerated myelin. In contrast, a substantial improvement of capillary morphology was detected in ALS mice receiving the high cell-dose treatment (**Figure 2Ae and Af**). Normal ultrastructural morphology of ECs and pericytes, adjacent astrocyte end-

feet, and preserved axonal myelin were noted. Just small areas of perivascular edema were seen.

Capillary morphology profiles in the lumbar spinal cords were similar to those in the cervical spinal cords. Control mice demonstrated a high percentage of capillaries with normal morphology (76.37 ± 2.55%) and a low percentage of moderately impaired capillaries (23.63 ± 2.55%) (**Figure 2B**). Severely damaged capillaries were not identified in control mice. Media-injected ALS mice showed a significant ($p = 0.001$) decrease of morphologically normal capillaries (24.20 ± 2.73%) and an increased percentage of moderately impaired capillaries (40.27 ± 1.78%) vs. controls. A high percentage of severely impaired capillaries (35.53 ± 2.86%) was determined in media mice (**Figure 2B**). Steadily increasing percentages of capillaries with normal morphology in correlation with increased cell doses were shown in cell-treated vs. media ALS mice: low dose - 21.17 ± 2.63%, mid dose - 28.20 ± 1.98%, and high dose - 53.47 ± 2.14% ($p = 0.001$). Of note, there was a significant increase of normal capillaries in mice receiving high cell-dose vs. low ($p = 0.001$) or mid ($p = 0.001$) cell dose treatment. The percentage of severely damaged microvessels gradually decreased as cell dosages increased: low dose - 31.67 ± 7.54%, mid dose - 20.20 ± 2.35%, and high dose - 9.63 ± 0.99% ($p = 0.003$) (**Figure 2B**). Of note, a smaller percentage of capillaries with severe impairment was noted in the lumbar spinal cords of mice treated with high cell-dose compared to results from cervical spinal cords (17.27 ± 4.75%) in the same animals. Similarly to the cervical spinal cord, increased percentages of capillaries with moderate morphological impairment were noted in low dose - 47.17 ± 8.69% and mid dose - 51.60 ± 4.29% vs. media mice with significant differences ($p = 0.011$ and $p = 0.003$, respectively) compared to controls. Only mice receiving the high cell-dose demonstrated a minor decrease of these moderately impaired capillaries (36.90 ± 3.06%) compared to media-treated animals (**Figure 2B**).

Together, results demonstrated severely compromised BSCB integrity in the cervical and lumbar spinal cords in media-treated ALS mice at 17 weeks of age, which is considered late symptomatic disease stage. Structural restoration of this barrier in the spinal cord was determined mainly in mice receiving the high hBM34+ cell dose and was confirmed by capillary morphology profiles.

### 3.2. Capillary permeability in the spinal cord

To confirm potential structural BSCB repair in symptomatic G93A mice by hBM34+ cell transplantation at different doses, functional vascular leakage was determined by quantitative analysis of EB extravasation into the spinal cord parenchyma of cell-treated, media-treated, and control mice at 17 weeks of age.

Photographs in **Figure 3** demonstrate control (**A**) and media-treated (**B**) mice in prone position after EB injection. There is a clear indication of dye penetration (blue color) under the skin due to fenestration of capillaries. Also, visible posterior lower, anterior thigh, and medial thigh muscle atrophy in left hindlimb of media mouse at 17 weeks of age can be observed (**Figure 3B**) compared to typical muscle condition in both hindlimbs of control mouse at the same age (**Figure 3B**). Quantitative analysis of EB extravasation into the spinal cord parenchyma showed significant ($p = 0.004$) dye tissue content in media-treated mice

(5.47 ± 0.85 μg/g) compared to controls (1.88 ± 0.44 μg/g) (**Figure 3C**). Although less EB extravasation was determined in the spinal cords of mice receiving the low (3.43 ± 0.62 μg/g) or mid (3.16 ± 1.01 μg/g) cell dose, there were no significant differences vs. media mice. In contrast, EB extravasation was significantly ($p = 0.022$) reduced in spinal cords of ALS mice receiving the high cell dose (2.43 ± 0.54 μg/g) (**Figure 3C**). Quantification of EB concentration in sera was performed as a control for spinal cord EB extravasation and showed no significant differences in EB levels in sera between control, media-treated, and cell-treated mice, confirming the same dye content in animals' blood after intravenous injection (**Figure 3D**).

Microvascular EB leakage was analyzed in the cervical and lumbar spinal cords from cell-treated, media-treated, and control mice. In the cervical spinal cord, EB was clearly detected within capillary lumen in the ventral horn (**Figure 4A and a**), dorsal horn (**Figure 4B and b**), and anterior white matter (**Figure 4C and c**) from control mice at 17 weeks of age. Vascular leakage of EB was distinguished in the ventral horn (**Figure 4D and D'**), dorsal horn (**Figure 4E and E'**), and anterior white matter (**Figure 4F and F'**) from media-treated animals of the same age. Of note, extravasated EB was observed at some distance from capillaries in the ventral (**Figure 4D**) and dorsal (**Figure 4E**) spinal horns of these mice. ALS mice receiving the low cell dose showed notable EB capillary leakage in the ventral horn (**Figure 4G and G'**), dorsal horn (**Figure 4H and H'**), and anterior white matter (**Figure 4I and I'**). Microvessels less permeable for EB were determined in analyzed spinal cord areas (**Figure 4J-L'**) from mice treated with mid cell dose. Considerable reductions of leaky capillaries in the ventral horn (**Figure 4M and M'**), dorsal horn (**Figure 4N and N'**), and anterior white matter (**Figure 4O and O'**) were detected in ALS mice after receiving the high cell dose. In the lumbar spinal cord, EB dye was observed intravascularly in the ventral horn (**Figure 5A and a**), dorsal horn (**Figure 5B and b**), and anterior white matter (**Figure 5C and c**) from control mice, similarly to cervical spinal cord findings. Substantial diffusion of EB into the spinal cord parenchyma from many blood vessels was detected in the ventral horn (**Figure 5D and D'**), dorsal horn (**Figure 5E and E'**), and anterior white matter (**Figure 5F and F'**) from media-treated mice. Analogous EB extravasation was seen in analyzed spinal cord areas from mice treated with low (**Figure 5G-I'**) or mid (**Figure 5J-L'**) cell dose. Lessened capillary permeability was demonstrated in the ventral horn (**Figure 5M and M'**), dorsal horn (**Figure 5N and N'**), and anterior white matter (**Figure 5O and O'**) from the high cell-treated mice.

Thus, structural improvement of microvasculature identified in the cervical and lumbar spinal cords via EM mainly in ALS mice receiving the high hBM34+ cell dose was confirmed by *functional* capillary status for EB leakage in animals treated with the same high cell-dose.

### 3.3. Immunohistochemical analysis of laminin in the spinal cord

Immunohistochemical analysis of laminin, a major component of the basal lamina, was performed in the cervical and lumbar spinal cords of cell-treated, media-treated, and control mice at 17 weeks of age to evaluate capillary integrity. Immunofluorescent staining for laminin demonstrated well organized microvasculature networks in the cervical (**Figure**

**6Aa**) and lumbar (**Figure 6Af**) ventral horns of control mice. In these animals, spinal cord capillaries displayed a continuous layer of laminin (**Figure 6Aa'and Af'**). Marked reduction of laminin immunoexpression in microvessels was determined in both cervical (**Figure 6Ab**) and lumbar (**Figure 6Ag**) spinal cords of media-treated ALS mice. At high magnification, irregularities of capillary laminin staining were obvious in the ventral horn in the cervical (**Figure 6Ab'**) and lumbar (**Figure 6Ag'**) spinal cords. ALS mice receiving the low cell dose showed a similar pattern of laminin immunoexpression in the spinal cords (cervical: **Figure 6Ac and Ac'**; lumbar: **Figure 6Ah and Ah'**) as in media mice. Increased numbers of capillaries with adequate laminin expression were observed in the cervical and lumbar spinal cords of micetreated with mid (cervical: **Figure 6Ad and Ad'**; lumbar: **Figure 6Ai and Ai'**) and high (cervical: **Figure 6Ae and Ae'**; lumbar: **Figure 6Aj and Aj'**) cell doses. Of note, more robust capillary laminin staining was apparent after the high cell-dose treatment (cervical: **Figure 6Ae'**; lumbar: **Figure 6Aj'**) vs. mid cell-dose.

Quantitative analysis of laminin immunoexpression presented as averages of ventral gray matter of the cervical and lumbar spinal cords in both sides confirmed the above description of laminin immunostaining in cell-treated, media-treated, and control mice. In the cervical spinal cord, media-treated mice showed a significant ($p = 0.001$) reduction of protein expression vs. controls (**Figure 6B**). There were no significant differences between the low cell-dose treatment and media mice. Yet, mice receiving the mid and high celldoses demonstrated significant ($p = 0.001$) increases of laminin immunoexpression vs. media-treated or low cell-treated animals (**Figure 6B**). In the lumbar spinal cord, a significant ($p = 0.001$) decrease of laminin detection was determined in media mice (**Figure 6C**), similarly to the cervical spinal cord. Although no significant differences were found in mice receiving the low cell-dose compared to media, significantly ($p = 0.001$) elevated laminin immunostaining was detected in mice treated with the mid and high cell-doses vs. media and low cell-dose (**Figure 6C**). Interestingly, high cell-dose mice showed a significantly ($p =0.008$) higher percentage of laminin expression compared to mid cell-dose treated animals.

Together, results demonstrated significant reduction and disruption of laminin immunoexpression in capillaries of the cervical and lumbar spinal cords in media-treated ALS mice at 17 weeks of age, suggesting compromised basement membrane integrity in these late symptomatic mice. The enhancement of laminin immunostaining in the spinal cord was determined in mice receiving the mid and high hBM34+ cell doses and was confirmed by quantitative analysis of this protein.

### 3.4. Immunocytochemical analysis of transplanted hBM34+ cells in blood smears

For identification of intravenously transplanted hBM34+ cells within blood circulation, immunofluorescent staining with the human-specific nuclei marker (HuNu) was performed in blood smears. Also, same immunostaining was applied for hBM34+ cell smears as control. Results demonstrated positive HuNu immunoexpression in all hBM34+ cells (**Figure 7A**). In blood smears from ALS mice receiving the high cell-dose, some cells were positive for the HuNu marker (**Figure 7B**). Counts of immunopositive cells for HuNu in all blood smears showed that these cells comprised $12.18 \pm 1.86\%$ of total nucleated cells.

There was no detection of human cells in blood smears from media-treated mice (**Figure 7C**).

### 3.5. Histological analysis of myelin and capillary density in the lumbar spinal cord

Morphological analyses of axonal myelin sheaths were performed in lateral funiculus (LF) and ventral horn (VH) on both sides of the lumbar spinal cords from cell-treated, media-treated, and control mice at 17 weeks of age. Also, capillary density was measured on both sides of the lumbar ventral horn. Results demonstrated well myelinated axons in LF and VH of control mice (**Figure 8A**). Typical motor neurons and capillaries were observed in VH of these mice. Media-treated ALS mice showed substantial decreases of myelin intensity in LF and VH (**Figure 8B**). In VH of media mice, motor neurons were reduced in size or degenerated. Capillary amounts in media-treated animals appeared to increase. Myelinated axons in LF of low (**Figure 8C**) and mid (**Figure 8D**) cell-dose treated mice were seen to moderately increase compared to media mice. Motor neurons in these treated mice were morphologically adequate. A high number of capillaries was detected in VH of these cell-treated animals. Dilated capillaries were noted (**Figure 8C**). ALS mice receiving the high cell-dose showed substantial enhancements of myelin in LF and VH (**Figure 8E**) similar to controls. Capillary numbers in VH seemed to decrease.

Quantitative analyses of myelin intensity presented in LF and VH of the lumbar spinal cords on both sides confirmed the above description of myelin staining in cell-treated, media-treated, and control mice.

Media-treated ALS mice showed a significant ($p = 0.001$) decrease of myelin (29.23 ± 2.38%) in LF on one side of the lumbar spinal cord compared to control mice (46.86 ± 2.16%) (**Figure 9A**). There were no significant differences in myelin expressions in LF between the low or mid cell-dose treated mice vs. media. In contrast, mice treated with the high cell-dose demonstrated significantly ($p = 0.001$) increased percentages of myelinated axons in LF on both sides of the lumbar spinal cords (side 1 – 47.77 ± 2.69%, side 2 – 55.15 ± 2.85%) compared to media-treated mice (side 1 – 29.23 ± 2.38%, side 2 – 41.29 ± 2.91%). Myelin intensity profile in VH was similar to LF. Significant ($p = 0.001$) decreases of myelin staining were determined in VH of media mice on both sides (side 1 – 3.34 ± 0.28%, side 2 – 4.61 ± 0.32%) vs. controls (side 1 – 9.28 ± 0.97%, side 2 – 9.68 ± 0.99%) (**Figure 9B**). Although non-significant differences were found in VH myelin of the low or mid cell-dose treated mice vs. media, a trend towards increased myelin expression was noted in mice after the high cell-dose treatment. Quantitative analyses of capillary density in VH also supported our observation in Figure 8. Capillary densities in media-treated animals were significantly ($p = 0.001$) higher on both sides of the lumbar spinal cord (side 1 – 734.48 ± 57.44 number/$mm^2$, side 2 – 820.98 ± 45.99 number/$mm^2$) vs. controls (side 1 – 236.62 ± 11.80 number/$mm^2$, side 2 – 275.39 ± 11.42 number/$mm^2$) (**Figure 9C**). Continued elevations of capillary density were also noted on both sides of VH in low and mid cell-dose treated compare to media ALS mice. However, significant decreases of capillary density were determined in mice receiving the high cell-dose (side 1 – 703.81 ± 59.54 number/$mm^2$, $p = 0.035$; side 2 – 717.26 ± 48.42 number/$mm^2$, $p = 0.007$) vs. mid celldose treated animals (side 1 – 975.55 ± 57.22 number/$mm^2$, side 2 – 1029.69 ± 75.29 number/$mm^2$) (**Figure 9C**).

Thus, substantial decreases of myelin intensity in LF and VH on both sides of the lumbar spinal cord were determined in media-treated ALS mice at 17 weeks of age, suggestive of axonal myelin sheath disintegration or even axonal degeneration in these late symptomatic mice. Significant enhancement of myelin expressions was mainly determined in LF of mice receiving the high cell-dose. Also, a significant increase of capillary density was noted in VH of media mice. Only mice treated with the high hBM34+ cell-dose showed significant decreases of capillary numbers on both sides of VH vs. mid cell-dose treatment.

## 4. Discussion

The present study evaluated the effects of intravenously administrated unmodified human bone marrow CD34+ (hBM34+) cells at different doses into symptomatic G93A SOD1 mice on structural and functional capillary repair in spinal cords. Furthermore, morphological axonal myelin coherence and capillary density were examined in the spinal cords as secondary therapeutic outcomes. The major study findings revealed that the high hBM34+ cell dose significantly: (1) restored capillary ultrastructure; (2) decreased capillary permeability for EB; (3) improved the basement membrane laminin integrity; (4) enhanced axonal myelin expressions in lateral funiculus; and (5) stabilized capillary density. Although some of the above benefits were demonstrated in the mid cell-dose (5 × 105 cells) treated mice, structural and functional improvements of microvasculature in the cervical and lumbar spinal cords were mainly determined in ALS mice receiving the high dose of 1 × 106 hBM34+ cells. These novel findings provide evidence that unmodified bone marrow hematopoietic stem cell treatment at optimal dose may be beneficial for repair of the damaged BSCB in the spinal cord in advanced stage of ALS, leading to the enhanced motor neuron survival and delayed disease progression as we reported previously (Garbuzova-Davis et al., 2017). In support of our treatment, umbilical cord blood-derived CD34+ cells have also proven effective for traumatic brain injury by stimulating angiogenesis and neurogenesis (Chen et al., 2014). Also, combining stem cell therapy with factors for enhancing the endogenous restorative mechanisms of the injured brain may be a promising therapeutic approach. It has been shown that post-stroke rats treated by combination of G-CSF and syngeneic bone marrowderived mesenchymal stem cells (Balseanu et al., 2014) or mononuclear cells (Buga et al., 2015) improved neurological function. Although, this treatment paradigm did not decrease infarct volume in rats, robust angiogenesis was detected in the infarct core. However, advantages of adult-derived stem cells for treatment of various neurodegenerative diseases have been discussed (Sanberg et al., 2012).

Our early study results (Garbuzova-Davis et al., 2007a, 2007b) demonstrated compromised BSCB integrity in the cervical and lumbar spinal cords in G93A SOD1 mice at 17 weeks of age. Primarily, abnormal endothelial cell (EC) morphology, degenerated astrocyte end-feet, and perivascular edema were evidenced in these late staged ALS mice via electron microscopy (Garbuzova-Davis et al., 2007a). Similarly, severe ultrastructural EC alterations in the spinal cords were shown in symptomatic G93A SOD1 rats (Nicaise et al., 2009). Results of the current study confirmed these previous observations in ALS mice and, moreover, a high percentage of severely impaired capillaries was determined in the spinal cords of media-treated mice at the late symptomatic stage. Substantial improvement of capillary ultrastructure and significant decrease in the percentage of severely damaged

microvessels in the cervical/lumbar spinal cords were most commonly detected in mice treated with the high cell dose. Thus, structural characteristics and morphological profiles of capillary integrity strongly support the effectiveness of hematopoietic stem cell transplantation for BSCB restoration in ALS.

Based on our recent report (Garbuzova-Davis et al., 2017), transplanted hBM34+ cells into symptomatic ALS mice differentiated into ECs and engrafted into numerous spinal cord capillaries of ALS mice primarily treated with the high cell dose, leading to a reduction of EB extravasation into the spinal cord parenchyma in these mice. Since this study was limited to determining capillary permeability only in mice receiving the high cell dose, the current investigation was extended to evaluate microvessel leakage for EB in animals treated with low and mid cell-doses. Data from the present study confirmed our previous finding and showed a significant decrease of EB extravasation into the spinal cord parenchyma of high cell-dose treated mice vs. media-treated animals. However, non-significant decreases of capillary leakage for EB were detected in mice receiving the low or mid cell-dose, suggesting that insufficient number of transplanted cells provide inadequate capillary coverage, which concurs with our previous study results (Garbuzova-Davis et al., 2017). This possibility was also supported by observation of EB extravasation into various areas of the spinal cord parenchyma. Notable capillary leakage for EB was detected not only in the ventral horn, but also in dorsal horn and anterior white matter of the cervical and lumbar spinal cords from ALS mice treated with the low or mid cell-dose. Pervasive permeability of microvessels, even at some distance from capillaries, in the spinal cord areas such as the ventral horn, dorsal horn, and anterior white matter determined in media-treated mice at 17 weeks of age is a novel finding indicating severe BSCB damage in ALS. Some study results suggest vascular damage as an early ALS pathological event based on evidence of BSCB alterations in SOD1 mutant mice and rats prior to motor neuron degeneration and neuroinflammation (Miyazaki et al., 2011; Nicaise et al., 2009; Zhong et al., 2008). It is possible that a dysfunctional BSCB is an initiating pathological trigger for ALS and prolonged barrier damage might accelerate motor neuron degeneration. However, our study detected barrier status only in the spinal cords. Nicaise et al. (Nicaise et al., 2009) demonstrated significant increases of EB extravasation into the spinal cord and brainstem tissues, but not in the brain, of symptomatic G93A SOD1 rats. Additional studies should be performed to determine pre- and post-transplant BBB status in the motor cortex and brainstem of ALS mice to determine the extent of B-CNS-B damage and potential repair. Another limitation of the current study is that EC competence was not fully examined. Dysfunction of tight junction proteins (ZO-1, occludin, and claudin-5) compromising BBB/BSCB integrity, resulting in vascular leakage, has been detected in the lumbar spinal cords of pre-symptomatic and symptomatic ALS mice (Miyazaki et al., 2011; Zhong et al., 2008). The expression of these tight junction proteins is currently under investigation to confirm BSCB restoration after hBM34+ cell transplantation at different doses and our study results will be reported in an upcoming paper.

Capillary basement membrane consistency is imperative for proper maintenance of microvessel integrity (Abbott et al., 2010; Pardridge, 1999). Marked reduction of laminin, a major non-collagenous basement membrane glycoprotein, was observed in both the cervical and lumbar spinal cords of symptomatic G93A mice, suggesting “loss of vascularization or

disruption of vascular basement membrane integrity" (Garbuzova-Davis et al., 2007b). Also, agrin, another basement membrane component, was noted to decrease in a G93A SOD1 rat model of ALS only at symptomatic stage (Nicaise et al., 2009). In the present study, a significant decrease of laminin immunostaining and irregular laminin patterning in capillary walls was determined in the ventral horns of the cervical and lumbar spinal cords in media-treated mice at 17 weeks of age, confirming our previous results (Garbuzova-Davis et al., 2007b). Although adequate laminin immunoexpression was observed in spinal cord capillaries of mid cell-dose treated mice, more robust protein staining was detected in mice after the high cell-dose treatment. Our data showed that the basement membrane integrity was enhanced with cell transplantation of the high dose, proving *structural* BSCB restoration by this cell treatment dosage. Other major findings of the study included substantial reductions of myelin intensity in the lateral funiculus (LF) and ventral horn (VH) of the lumbar spinal cord in media-treated ALS mice at 17 weeks of age. These data suggest axonal myelin sheath disintegration or even axonal degeneration in these symptomatic mice, confirming our previous ultrastructural observation (Garbuzova-Davis et al., 2007a) of extensive losses of axonal myelinization in the brainstem, cervical and lumbar spinal cords of G93A mice at late stage of disease. Also, massive myelin disorganization in the spinal cords from G93A SOD1 rats was most pronounced in paralyzed animals (Niebroj-Dobosz et al., 2007). Importantly, a significant decrease of myelin staining in this study was detected in LF on one side of the lumbar spinal cord. Typically, G93A SOD1 mice show initial motor function impairment due to muscle weakness, leading to muscle atrophy and paralysis, in one hindlimb (see Figure 3B), and later both hindlimbs and/or forelimbs are involved during disease progression. Determining less myelin mainly in lateral white matter on one side of the lumbar spinal cord may indicate impairment of crossed descending (corticospinal and rubrospinal) and ascending (spinothalamic) spinal cord tracts accordingly to location of these tracts in mice (Watson and Harrison, 2012). It has been shown that degeneration of white matter tracts begin in G93A SOD1 mice at 16 weeks of age via axonal pathology (King et al., 2012) and later progressive loss of descending corticospinal, bulbospinal, and rubrospinal tracts was noted (Zang and Cheema, 2002). Deterioration of spinal cord pathways may be initiated by motor neuron dysfunction, reflecting the significant reduction of myelin in the lumbar ventral horn demonstrated in our study. There are two contradictory hypotheses regarding motor neuron death in ALS. According to the "dying-forward" hypothesis (Browne et al., 2006; Eisen et al., 1992), initial dysfunction occurs in the corticomotor neurons mediating anterograde degeneration of lower motor neurons by glutamate excitotoxicity in ALS. In contrast, the "dyingback" hypothesis states that the nerve terminals and motor neuron junctions are degraded prior to motor neuron degeneration (Dadon-Nachum et al., 2011). However, axonal degeneration is thought to precede motor neuron death since retrograde axonal transport of trophic factors is showed to impair in G93A mice even prior to motor neuron loss (Bilsland et al., 2010; Fischer and Glass, 2007). We believe that both hypotheses could be valid for somatic degeneration of the low motor neurons due to axonopathy and/or neuropathy via direct influence of various intrinsic and/or extrinsic factors. However, Lingor et al. (Lingor et al., 2012) noted that "the mechanisms of neuronal cell body demise must differ from axonal degeneration and the latter cannot be explained as a pure consequence of the somatic dysfunction". Despite pathological mechanisms contributing to motor neuron degeneration in ALS, significant increases of

motor neuron survival (Garbuzova-Davis et al., 2017) and myelin expressions in LF in the lumbar spinal cord in symptomatic ALS mice shown in the present study were mainly determined in mice treated with the high hBM34+ cell-dose. However, the involvement of oligodendrocytes in post-transplant enhancement of axonal myelination should be addressed. It has been shown that oligodendrocytes are dysfunctional in ALS (Cui et al., 2014; Ferraiuolo et al., 2016; Nonneman et al., 2014; Rohan et al., 2014), resulting in potential detrimental effects on myelin production and motor neuron degeneration. Moreover, iron and myelin disturbances in white matter were found in ALS patients and correlated with disease severity through susceptibility-weighted imaging (Prell et al., 2015). Additionally, myelin changes were determined within the anterior corpus callosum and frontal lobe of ALS patients compared to the widespread reduction of cerebral myelin water fraction in patients with primary lateral sclerosis determined via MRI sequence method (Kolind et al., 2013). Thus, determining the role of oligodendrocytes in terms of maintaining myelin homeostasis may be required to confirm the mechanisms underlying our proposed cell treatment and will be investigated in the near future.

Finally, our examination of capillary density in the lumbar ventral horn demonstrated a significant increase in media-treated ALS mice at the late symptomatic disease stage compared to controls. These data supported our previous study report showing substantial escalation of microvascular density in the lumbar spinal cords from sporadic ALS patients, suggesting that “neovascularization may occur in areas of motor neuron degeneration to compensate for dysfunctional capillaries” (Garbuzova-Davis et al., 2012a). Supporting this finding, transplantation of bone marrow-derived CD34+ cells enhanced neovascularization in treatment of bone fracture in a rat model (Kawakami et al., 2012). In contrast, others have shown 10–15% reductions in total capillary length in the lumbar spinal cords of pre-symptomatic SOD1 mutants (Zhong et al., 2008) and lower capillary density via PECAM-1 staining in the spinal gray matter of G93A mice with disease progression, suggesting a reduction of spinal cord microcirculation (Miyazaki et al., 2011). Although the reduced microcirculation supports observations of a 30–45% decrease in blood flow through the spinal cord (Zhong et al., 2008), discrepancies between our data and others regarding capillary length and/or density may warrant further investigation. Improved techniques and methodologies could be advantageous to clarify these important data. Despite contradictory results, the present study showed a significant increase of capillary density in the lumbar ventral horn in media-treated ALS mice at 17 weeks of age, potentially indicating compensatory formation of new vessels to provide needed nutrients and oxygen for dying motor neurons. However, this suggestion still needs confirmation. In mice treated with low or mid cell-doses, continued elevation of capillary density was also noted on both sides of lumbar ventral horn, likely due to insufficient numbers of transplanted cells. In contrast, a substantial decrease in density of microvessels was demonstrated in ALS mice after the high hBM34+ cell-dose treatment. Possibly, structural and functional restoration of BSCB in these mice prompted capillary stabilization in the spinal cord at 4 weeks post-transplantation. One neuroprotective mechanism of a restored BSCB may be the blocking entry of pro-inflammatory monocyte/macrophage cells. Also, detection of transplanted cells in blood circulation by HuNu marker suggest the potential for ongoing barrier repair supporting regenerative processes towards establishment of BSCB integrity in ALS.

## 4. Conclusion

The present study demonstrated that unmodified human bone marrow CD34+ (hBM34+) cells intravenously administrated into symptomatic G93A SOD1 mice dose-dependently improve structural and functional BSCB repair in the spinal cord. Restoration of ultrastructural capillary morphology, reduction of capillary permeability, improvement of basement membrane integrity, enhancement of axonal myelin coherence, and stabilization of capillary density in the cervical and lumbar spinal cords were primarily determined in ALS mice receiving the high dose of 1 × 106 cells. These beneficial effects were potentially achieved via replacement of damaged endothelial cells with newly introduced cells, a likelihood which is supported by our previous study results showing that transplanted stem cells differentiated into endothelial cells and engrafted within numerous spinal cord capillaries. However, the administered cells could additionally provide endogenous repair of endothelial cells in ALS by secretion of specific angiogenic factors; this possibility is currently under investigation. Moreover, repeated cell administrations with smaller doses might substantially contribute to ongoing replacement or endogenous repair of damaged endothelial cells over the course of the disease. Additionally, transplantation of cells from a restricted lineage, such as endothelial progenitors, may provide superior restoration of the damaged BSCB in ALS, which we are presently pursuing. Furthermore, since the present study focused on BSCB integrity at 4 weeks post-transplant, evaluating the effect of cell treatment for a longer post-injection period, especially on mouse lifespan, is important. This study is currently underway. Although various studies should be conducted to evaluate advantages of cell therapy for barrier repair, results of the present study provide evidence that unmodified bone marrow hematopoietic stem cell treatment at optimal dose might be beneficial for repair of the damaged BSCB in the spinal cord in advanced stage of ALS.

## Acknowledgements

This study was supported by the NIH, NINDS (1R01NS090962) grant. We would like to acknowledge staff, including veterinarians, from USF's Division of Comparative Medicine for their substantial assistance in animal care and surgical procedures. We also gratefully acknowledge Donna Morrison and Inger Mills for their assistance and support of the studies.

## References

Abbott NJ, Patabendige AAK, Dolman DEM, Yusof SR, Begley DJ, 2010 Structure and function of the blood-brain barrier. Neurobiol. Dis 37, 13–25. 10.1016/j.nbd.2009.07.030 [PubMed: 19664713]

Ay I, Francis JW, Brown RH, Jr, 2008 VEGF increases blood-brain barrier permeability to Evans blue dye and tetanus toxin fragment C but not adeno-associated virus in ALS mice. Brain Res. 1234, 198–205. 10.1016/j.brainres.2008.07.121 [PubMed: 18725212]

Balseanu AT, Buga A-M, Catalin B, Wagner D-C, Boltze J, Zagrean A-M, Reymann K, Schaebitz W, Popa-Wagner A, 2014 Multimodal Approaches for Regenerative Stroke Therapies: Combination of Granulocyte Colony-Stimulating Factor with Bone Marrow Mesenchymal Stem Cells is Not Superior to G-CSF Alone. Front Aging Neurosci 6, 130 10.3389/fnagi.2014.00130 [PubMed: 25002846]

Bataveljić D, Djogo N, Zupunski L, Bajić A, Nicaise C, Pochet R, Bacić G, Andjus PR, 2009 Live monitoring of brain damage in the rat model of amyotrophic lateral sclerosis. Gen. Physiol. Biophys 28 Spec No, 212–218. [PubMed: 19893103]

Bataveljic D, Milosevic M, Radenovic L, Andjus P, 2014 Novel molecular biomarkers at the blood-brain barrier in ALS. Biomed. Res. Int 2014, 907545 10.1155/2014/907545 [PubMed: 24949481]

Bataveljic D, Nikolić L, Milosević M, Todorović N, Andjus PR, 2012 Changes in the astrocytic aquaporin-4 and inwardly rectifying potassium channel expression in the brain of the amyotrophic lateral sclerosis SOD1(G93A) rat model. Glia 60, 1991–2003. 10.1002/glia.22414 [PubMed: 22987392]

Bilsland LG, Sahai E, Kelly G, Golding M, Greensmith L, Schiavo G, 2010 Deficits in axonal transport precede ALS symptoms in vivo. Proc. Natl. Acad. Sci. U.S.A 107, 20523–20528. [PubMed: 21059924]

10.1073/pnas.1006869107

Browne SE, Yang L, DiMauro J-P, Fuller SW, Licata SC, Beal MF, 2006 Bioenergetic abnormalities in discrete cerebral motor pathways presage spinal cord pathology in the G93A SOD1 mouse model of ALS. Neurobiol. Dis 22, 599–610. 10.1016/j.nbd.2006.01.001 [PubMed: 16616851]

Buga A-M, Scheibe J, Moller K, Ciobanu O, Posel C, Boltze J, Popa-Wagner A, 2015 Granulocyte colony-stimulating factor and bone marrow mononuclear cells for stroke treatment in the aged brain. Curr Neurovasc Res 12, 155–162. [PubMed: 25760217]

Calvo AC, Manzano R, Mendonça DMF, Muñoz MJ, Zaragoza P, Osta R, 2014 Amyotrophic lateral sclerosis: a focus on disease progression. Biomed. Res. Int 2014, 925101 10.1155/2014/925101 [PubMed: 25157374]

Chen S-H, Wang J-J, Chen C-H, Chang H-K, Lin M-T, Chang F-M, Chio C-C, 2014 Umbilical cord blood-derived $CD34^+$ cells improve outcomes of traumatic brain injury in rats by stimulating angiogenesis and neurogenesis. Cell Transplant. 23, 959–979. 10.3727/096368913X667006 [PubMed: 23582375]

Cleveland DW, Rothstein JD, 2001 From Charcot to Lou Gehrig: deciphering selective motor neuron death in ALS. Nat. Rev. Neurosci 2, 806–819. 10.1038/35097565 [PubMed: 11715057]

Cui Y, Masaki K, Yamasaki R, Imamura S, Suzuki SO, Hayashi S, Sato S, Nagara Y, Kawamura MF, Kira J, 2014 Extensive dysregulations of oligodendrocytic and astrocytic connexins are associated with disease progression in an amyotrophic lateral sclerosis mouse model. J. Neuroinflammation 11, 42 10.1186/1742-2094-11-42 [PubMed: 24597481]

Dadon-Nachum M, Melamed E, Offen D, 2011 The “dying-back” phenomenon of motor neurons in ALS. J. Mol. Neurosci 43, 470–477. 10.1007/s12031-010-9467-1 [PubMed: 21057983]

D’Amico E, Factor-Litvak P, Santella RM, Mitsumoto H, 2013 Clinical perspective on oxidative stress in sporadic amyotrophic lateral sclerosis. Free Radic. Biol. Med 65, 509–527. 10.1016/j.freeradbiomed.2013.06.029 [PubMed: 23797033]

Di Scipio F, Raimondo S, Tos P, Geuna S, 2008 A simple protocol for paraffin-embedded myelin sheath staining with osmium tetroxide for light microscope observation. Microsc. Res. Tech 71, 497–502. 10.1002/jemt.20577 [PubMed: 18320578]

Eisen A, Kim S, Pant B, 1992 Amyotrophic lateral sclerosis (ALS): a phylogenetic disease of the corticomotoneuron? Muscle Nerve 15, 219–224. 10.1002/mus.880150215 [PubMed: 1549143]

Eve DJ, Steiner G, Mahendrasah A, Sanberg PR, Kurien C, Thomson A, Borlongan CV, GarbuzovaDavis S, 2018 Reduction of microhemorrhages in the spinal cord of symptomatic ALS mice after intravenous human bone marrow stem cell transplantation accompanies repair of the blood-spinal cord barrier. Oncotarget 9, 10621–10634. https://doi.org/10.18632/oncotarget.24360 [PubMed: 29535831]

Feirabend HK, Choufoer H, Ploeger S, 1998 Preservation and staining of myelinated nerve fibers. Methods 15, 123–131. 10.1006/meth.1998.0615 [PubMed: 9654459]

Ferraiuolo L, Meyer K, Sherwood TW, Vick J, Likhite S, Frakes A, Miranda CJ, Braun L, Heath PR, Pineda R, Beattie CE, Shaw PJ, Askwith CC, McTigue D, Kaspar BK, 2016 Oligodendrocytes contribute to motor neuron death in ALS via SOD1-dependent mechanism. Proc. Natl. Acad. Sci. U.S.A 113, E6496–E6505. 10.1073/pnas.1607496113 [PubMed: 27688759]

Fischer LR, Glass JD, 2007 Axonal degeneration in motor neuron disease. Neurodegener. Dis 4, 431–442. 10.1159/000107704 [PubMed: 17934327]

Garbuzova-Davis S, Haller E, Saporta S, Kolomey I, Nicosia SV, Sanberg PR, 2007a Ultrastructure of blood-brain barrier and blood-spinal cord barrier in SOD1 mice modeling ALS. Brain Res. 1157, 126–137. 10.1016/j.brainres.2007.04.044 [PubMed: 17512910]

Garbuzova-Davis S, Haller E, Tajiri N, Thomson A, Barretta J, Williams SN, Haim ED, Qin H, Frisina-Deyo A, Abraham JV, Sanberg PR, Van Loveren H, Borlongan CV, 2016 Blood-Spinal Cord Barrier Alterations in Subacute and Chronic Stages of a Rat Model of Focal Cerebral Ischemia. J. Neuropathol. Exp. Neurol 75, 673–688. 10.1093/jnen/nlw040 [PubMed: 27283328]

Garbuzova-Davis S, Haller E, Williams SN, Haim ED, Tajiri N, Hernandez-Ontiveros DG, FrisinaDeyo A, Boffeli SM, Sanberg PR, Borlongan CV, 2014 Compromised blood-brain barrier competence in remote brain areas in ischemic stroke rats at chronic stage. J. Comp. Neurol 522, 3120–3137. 10.1002/cne.23582 [PubMed: 24610730]

Garbuzova-Davis S, Hernandez-Ontiveros DG, Rodrigues MCO, Haller E, Frisina-Deyo A, Mirtyl S, Sallot S, Saporta S, Borlongan CV, Sanberg PR, 2012a Impaired blood-brain/spinal cord barrier in ALS patients. Brain Res. 1469, 114–128. 10.1016/j.brainres.2012.05.056 [PubMed: 22750125]

Garbuzova-Davis S, Kurien C, Thomson A, Falco D, Ahmad S, Staffetti J, Steiner G, Abraham S, James G, Mahendrasah A, Sanberg PR, Borlongan CV, 2017 Endothelial and Astrocytic Support by Human Bone Marrow Stem Cell Grafts into Symptomatic ALS Mice towards Blood-Spinal Cord Barrier Repair. Sci. Rep 7, 884 10.1038/s41598-017-00993-0 [PubMed: 28408761]

Garbuzova-Davis S, Rodrigues MCO, Hernandez-Ontiveros DG, Louis MK, Willing AE, Borlongan CV, Sanberg PR, 2011 Amyotrophic lateral sclerosis: a neurovascular disease. Brain Res. 1398, 113–125. 10.1016/j.brainres.2011.04.049 [PubMed: 21632035]

Garbuzova-Davis S, Rodrigues MCO, Mirtyl S, Turner S, Mitha S, Sodhi J, Suthakaran S, Eve DJ, Sanberg CD, Kuzmin-Nichols N, Sanberg PR, 2012b Multiple intravenous administrations of human umbilical cord blood cells benefit in a mouse model of ALS. PLoS ONE 7, e31254 10.1371/journal.pone.0031254 [PubMed: 22319620]

Garbuzova-Davis S, Sanberg CD, Kuzmin-Nichols N, Willing AE, Gemma C, Bickford PC, Miller C, Rossi R, Sanberg PR, 2008a Human umbilical cord blood treatment in a mouse model of ALS: optimization of cell dose. PLoS ONE 3, e2494 10.1371/journal.pone.0002494 [PubMed: 18575617]

Garbuzova-Davis S, Sanberg PR, 2014 Blood-CNS barrier impairment in ALS patients versus an animal model. Front. Cell. Neurosci. 8, 21 10.3389/fncel.2014.00021 [PubMed: 24550780]

Garbuzova-Davis S, Saporta S, Haller E, Kolomey I, Bennett SP, Potter H, Sanberg PR, 2007b Evidence of compromised blood-spinal cord barrier in early and late symptomatic SOD1 mice modeling ALS. PLoS ONE 2, e1205 10.1371/journal.pone.0001205 [PubMed: 18030339]

Garbuzova-Davis S, Saporta S, Sanberg PR, 2008b Implications of blood-brain barrier disruption in ALS. Amyotroph. Lateral Scler 9, 375–376. 10.1080/17482960802160990 [PubMed: 18608097]

Garbuzova-Davis S, Willing AE, Zigova T, Saporta S, Justen EB, Lane JC, Hudson JE, Chen N, Davis CD, Sanberg PR, 2003 Intravenous administration of human umbilical cord blood cells in a mouse model of amyotrophic lateral sclerosis: distribution, migration, and differentiation. J. Hematother. Stem Cell Res 12, 255–270. 10.1089/152581603322022990 [PubMed: 12857367]

Gordon PH, 2011 Amyotrophic lateral sclerosis: pathophysiology, diagnosis and management. CNS Drugs 25, 1–15. 10.2165/11586000-000000000-00000

Henkel JS, Beers DR, Wen S, Bowser R, Appel SH, 2009 Decreased mRNA expression of tight junction proteins in lumbar spinal cords of patients with ALS. Neurology 72, 1614–1616. 10.1212/WNL.0b013e3181a41228 [PubMed: 19414730]

Hugon J, 1996 Riluzole and ALS therapy. Wiener medizinische Wochenschrift (1946) 146, 185–187. [PubMed: 8873431]

Kawakami Y, Ii M, Alev C, Kawamoto A, Matsumoto T, Kuroda R, Shoji T, Fukui T, Masuda H, Akimaru H, Mifune Y, Kuroda T, Horii M, Yokoyama A, Kurosaka M, Asahara T, 2012 Local Transplantation of Ex Vivo Expanded Bone Marrow-Derived CD34-Positive Cells Accelerates Fracture Healing. Cell Transplant. 21, 2689–2709. 10.3727/096368912X654920 [PubMed: 22943882]

Kiernan MC, Vucic S, Cheah BC, Turner MR, Eisen A, Hardiman O, Burrell JR, Zoing MC, 2011 Amyotrophic lateral sclerosis. Lancet 377, 942–955. 10.1016/S0140-6736(10)61156-7 [PubMed: 21296405]

King AE, Blizzard CA, Southam KA, Vickers JC, Dickson TC, 2012 Degeneration of axons in spinal white matter in G93A mSOD1 mouse characterized by NFL and α-internexin immunoreactivity. Brain Res. 1465, 90–100. 10.1016/j.brainres.2012.05.018 [PubMed: 22609817]

Kolind S, Sharma R, Knight S, Johansen-Berg H, Talbot K, Turner MR, 2013 Myelin imaging in amyotrophic and primary lateral sclerosis. Amyotroph. Lateral Scler. Frontotemporal Degener 14, 562–573. 10.3109/21678421.2013.794843 [PubMed: 23678852]

Kumar DR, Aslinia F, Yale SH, Mazza JJ, 2011 Jean-Martin Charcot: the father of neurology. Clin. Med. Res 9, 46–49. 10.3121/cmr.2009.883 [PubMed: 20739583]

Lingor P, Koch JC, Tönges L, Bähr M, 2012 Axonal degeneration as a therapeutic target in the CNS. Cell Tissue Res. 349, 289–311. 10.1007/s00441-012-1362-3 [PubMed: 22392734]

Martin LJ, Price AC, Kaiser A, Shaikh AY, Liu Z, 2000 Mechanisms for neuronal degeneration in amyotrophic lateral sclerosis and in models of motor neuron death (Review). Int. J. Mol. Med 5, 3–13. [PubMed: 10601567]

McCombe PA, Henderson RD, 2011 The role of immune and inflammatory mechanisms in ALS. Curr. Mol. Med 11, 246–254. [PubMed: 21375489]

Miller RG, Mitchell JD, Lyon M, Moore DH, 2003 Riluzole for amyotrophic lateral sclerosis (ALS)/ motor neuron disease (MND). Amyotroph. Lateral Scler. Other Motor Neuron Disord. 4, 191–206. [PubMed: 13129806]

Miyazaki K, Ohta Y, Nagai M, Morimoto N, Kurata T, Takehisa Y, Ikeda Y, Matsuura T, Abe K, 2011 Disruption of neurovascular unit prior to motor neuron degeneration in amyotrophic lateral sclerosis. J. Neurosci. Res 89, 718–728. 10.1002/jnr.22594 [PubMed: 21337372]

Nicaise C, Mitrecic D, Demetter P, De Decker R, Authelet M, Boom A, Pochet R, 2009 Impaired blood-brain and blood-spinal cord barriers in mutant SOD1-linked ALS rat. Brain Res. 1301, 152–162. 10.1016/j.brainres.2009.09.018 [PubMed: 19748495]

Niebroj-Dobosz I, Rafałowska J, Fidziańska A, Gadamski R, Grieb P, 2007 Myelin composition of spinal cord in a model of amyotrophic lateral sclerosis (ALS) in SOD1G93A transgenic rats. Folia Neuropathol. 45, 236–241. [PubMed: 18176898]

Nonneman A, Robberecht W, Van Den Bosch L, 2014 The role of oligodendroglial dysfunction in amyotrophic lateral sclerosis. Neurodegener. Dis. Manag 4, 223–239. 10.2217/nmt.14.21 [PubMed: 25095817]

Papadimitriou D, Le Verche V, Jacquier A, Ikiz B, Przedborski S, Re DB, 2010 Inflammation in ALS and SMA: sorting out the good from the evil. Neurobiol. Dis 37, 493–502. 10.1016/j.nbd. 2009.10.005 [PubMed: 19833209]

Pardridge WM, 1999 Blood-brain barrier biology and methodology. J. Neurovirol 5, 556–569. 10.3109/13550289909021285 [PubMed: 10602397]

Pratt AJ, Getzoff ED, Perry JJP, 2012 Amyotrophic lateral sclerosis: update and new developments. Degener. Neurol. Neuromuscul. Dis 2012, 1–14. 10.2147/DNND.S19803 [PubMed: 23019386]

Prell T, Hartung V, Tietz F, Penzlin S, Ilse B, Schweser F, Deistung A, Bokemeyer M, Reichenbach JR, Witte OW, Grosskreutz J, 2015 Susceptibility-weighted imaging provides insight into white matter damage in amyotrophic lateral sclerosis. PLoS ONE 10, e0131114 10.1371/journal.pone.0131114 [PubMed: 26110427]

Rodrigues MCO, Sanberg PR, Cruz LE, Garbuzova-Davis S, 2014 The innate and adaptive immunological aspects in neurodegenerative diseases. J. Neuroimmunol 269, 1–8. 10.1016/ j.jneuroim.2013.09.020 [PubMed: 24161471]

Rodrigues MCO, Voltarelli JC, Sanberg PR, Borlongan CV, Garbuzova-Davis S, 2012 Immunological aspects in amyotrophic lateral sclerosis. Transl. Stroke Res 3, 331–340. 10.1007/ s12975-012-0177-6 [PubMed: 24323808]

Rohan Z, Matej R, Rusina R, Kovacs GG, 2014 Oligodendroglial response in the spinal cord in TDP-43 proteinopathy with motor neuron involvement. Neurodegener. Dis 14, 117–124. 10.1159/000362929 [PubMed: 25115814]

Rothstein JD, 2017 Edaravone: A new drug approved for ALS. Cell 171, 725 10.1016/j.cell. 2017.10.011 [PubMed: 29100067]

Rothstein JD, 2009 Current hypotheses for the underlying biology of amyotrophic lateral sclerosis. Ann. Neurol 65 Suppl 1, S3–9. 10.1002/ana.21543 [PubMed: 19191304]

Sanberg PR, Eve DJ, Metcalf C, Borlongan CV, 2012 Advantages and challenges of alternative sources of adult-derived stem cells for brain repair in stroke. Prog. Brain Res 201, 99–117. 10.1016/B978-0-444-59544-7.00006-8 [PubMed: 23186712]

Sorarù G, Ermani M, Logroscino G, Palmieri A, D' Ascenzo C, Orsetti V, Volpe M, Cima V, Zara G, Pegoraro E, Angelini C, 2010 Natural history of upper motor neuron-dominant ALS. Amyotroph. Lateral Scler 11, 424–429. 10.3109/17482960903300867 [PubMed: 19929748]

Strong MJ, Kesavapany S, Pant HC, 2005 The pathobiology of amyotrophic lateral sclerosis: a proteinopathy? J. Neuropathol. Exp. Neurol 64, 649–664. [PubMed: 16106213]

Talbot K, 2009 Motor neuron disease: the bare essentials. Pract. Neurol 9, 303–309. 10.1136/jnnp.2009.188151 [PubMed: 19762894]

Watson C, Harrison M, 2012 The location of the major ascending and descending spinal cord tracts in all spinal cord segments in the mouse: actual and extrapolated. Anat. Rec (Hoboken) 295, 1692–1697. 10.1002/ar.22549

Wijesekera LC, Leigh PN, 2009 Amyotrophic lateral sclerosis. Orphanet J. Rare Dis 4, 3 10.1186/1750-1172-4-3 [PubMed: 19192301]

Winkler EA, Sengillo JD, Sullivan JS, Henkel JS, Appel SH, Zlokovic BV, 2013 Blood-spinal cord barrier breakdown and pericyte reductions in amyotrophic lateral sclerosis. Acta Neuropathol. 125, 111–120. 10.1007/s00401-012-1039-8 [PubMed: 22941226]

Zang DW, Cheema SS, 2002 Degeneration of corticospinal and bulbospinal systems in the superoxide dismutase 1(G93A G1H) transgenic mouse model of familial amyotrophic lateral sclerosis. Neurosci. Lett 332, 99–102. [PubMed: 12384220]

Zhao W, Beers DR, Appel SH, 2013 Immune-mediated mechanisms in the pathoprogression of amyotrophic lateral sclerosis. J. Neuroimmune Pharmacol 8, 888–899. 10.1007/s11481013-9489-x [PubMed: 23881705]

Zhong Z, Deane R, Ali Z, Parisi M, Shapovalov Y, O'Banion MK, Stojanovic K, Sagare A, Boillee S, Cleveland DW, Zlokovic BV, 2008 ALS-causing SOD1 mutants generate vascular changes prior to motor neuron degeneration. Nat. Neurosci 11, 420–422. 10.1038/nn2073 [PubMed: 18344992]

## Highlights

- Dose-dependent effect of transplanted hBM34+ cells was determined on BSCB repair.
- High cell-dose significantly improved ultrastructural capillary morphology.
- High cell-dose significantly reduced capillary permeability.
- High cell-dose enhanced axon/myelin coherence and capillary density.
- Optimal cell dose showed promise to repair damaged BSCB in advanced stage of ALS.

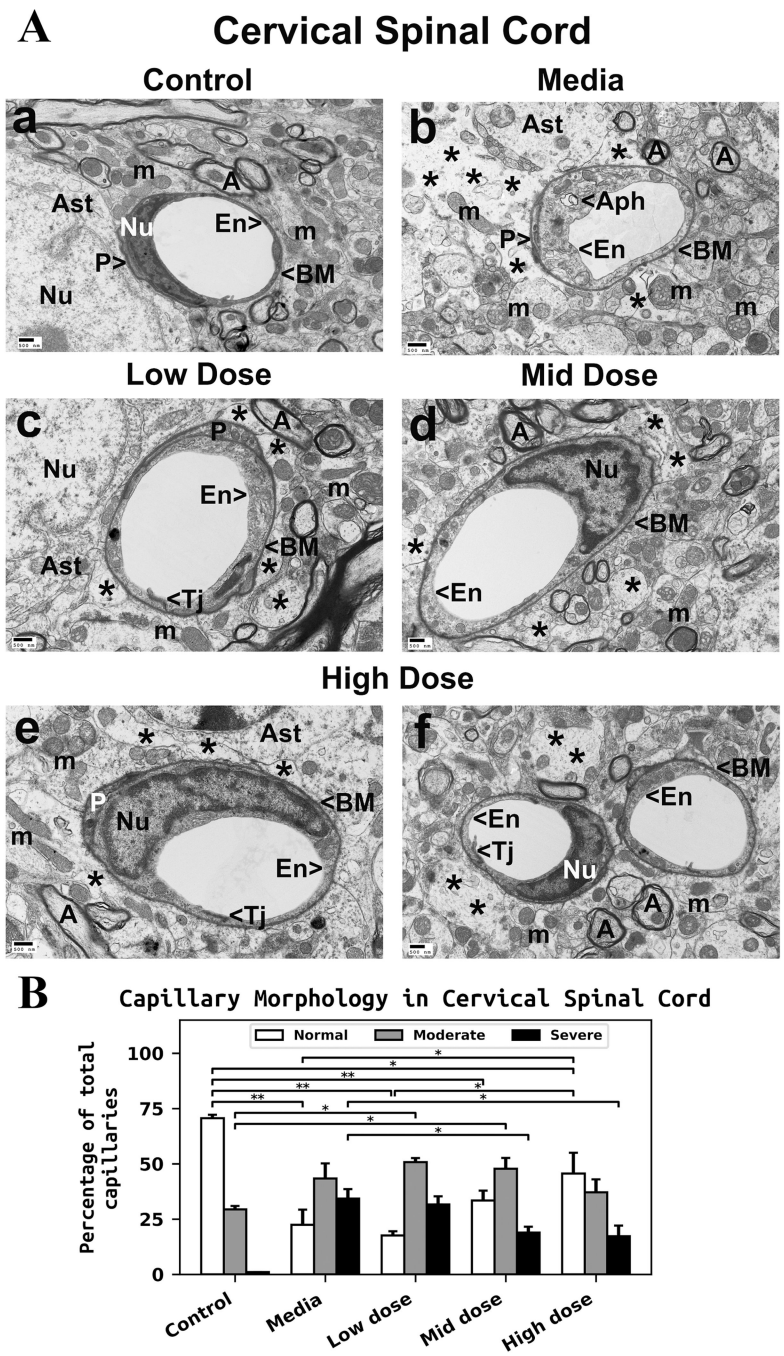


**Figure 1. Characteristics of capillary ultrastructure in the cervical spinal cord of G93A mice.**

**(A)** *Electron microscopy examination of microvasculature in the cervical ventral horn.* Control mouse showed typical ultrastructure of endothelium, neuropil, and axons **(Aa)**. Capillary consisted of an endothelial cell and a single layer of basement membrane. Mitochondria and myelinated axons were well preserved. **(Ab)** In media-treated mice at 17 weeks of age, swollen or vacuolated endothelial cells, degenerated astrocyte foot-processes, and extensive perivascular protein-filled edema were determined in numerous capillaries. Large autophagosome was found in cytoplasm of endothelial cell. Swollen free floating

mitochondria and degenerated myelinated axons were noted. **(Ac)** Mice receiving low cell dose showed swollen endothelia and perivascular edema. In some microvessels, astrocyte end-feet were adjacent to capillary wall. In mice receiving mid cell dose (**Ad**), near normal endothelium morphology and less perivascular edema were observed. A few axons with degenerated myelin were also detected in neuropil. **(Ae, Af)** Numerous capillaries demonstrated typical endothelium morphology in mice after treatment with high cell dose. Some areas of perivascular edema between capillary and astrocyte end-feet and degenerated myelinated axons were determined. En – endothelial cell, Tj – tight junction, BM – basement membrane, P - pericyte, Aph – autophagosome, Ast – astrocyte, A – axon, m – mitochondrion, Nu – nuclei, * - perivascular edema. Scale bar in a-f is 500 nm. **(B)** *Quantitative analysis of capillary morphology.* Control mice showed a high percentage of capillaries with normal morphology and low numbers of moderately impaired capillaries. Media mice demonstrated a significant decrease of morphologically normal capillaries, an increase of capillaries with moderate impairment, and a high percentage of severely damaged microvessels. Cell-treated mice displayed a gradual increase of capillaries with normal morphology consistent with cell dose. Percentage of severely compromised capillaries was significantly reduced in mice treated with mid or high cell dose. Increased percentages of capillaries with moderate impairment were noted only in low and mid-treated mice, but no significant differences were found compared to media animals. A slight decrease in moderately impaired capillaries was detected in high cell-treated mice vs. media. *$p < 0.05$, **$p < 0.01$.

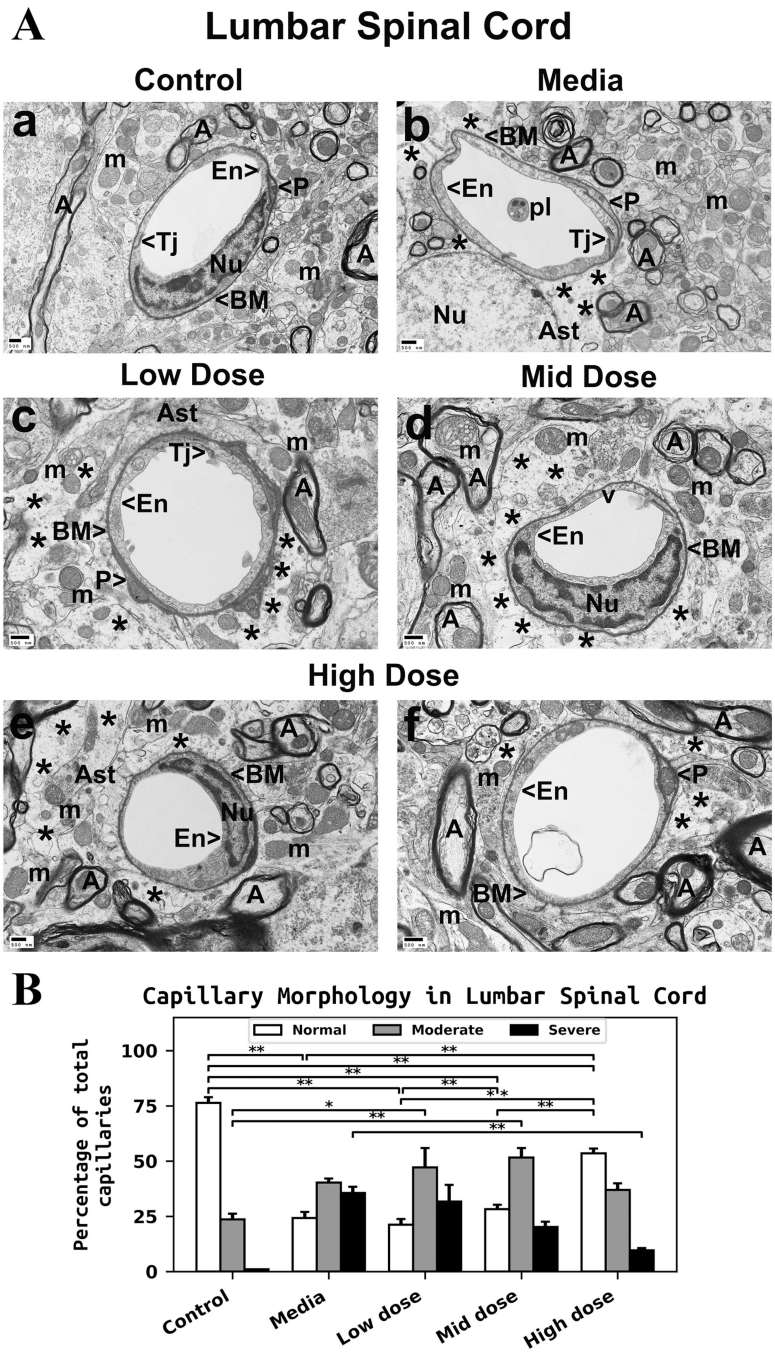


**Figure 2. Characteristics of capillary ultrastructure in the lumbar spinal cord of G93A mice.**

**(A)** *Electron microscopy examination of microvasculature in the lumbar ventral horn.* Control mouse demonstrated intact ultrastructural morphology of ventral horn capillaries **(Aa)**. Capillary consisted of typical endothelium composed of a single layer of endothelial cells, pericytes, tight junction, surrounding basement membrane, and adjacent astrocyte end-feet. Mitochondria and myelinated axons were well preserved in neuropil. **(Ab)** Mediatreated mice demonstrated degenerated endothelial cells and astrocyte foot-processes. Perivascular protein-filled edema was determined in numerous capillaries. Swollen

mitochondria were also observed in the neuropil and within axons. Myelin disruptions in surrounding axons were noted. ALS mice receiving the low or mid cell dose treatment demonstrated no improvement in capillary morphology. Swollen or vacuolated ECs in numerous capillaries were detected in low **(Ac)** or mid **(Ad)** cell dose treated mice. Significant perivascular edema was determined in these cell-treated mice. Mitochondria with disrupted cristae were seen in axon **(**top left, **Ad)** in addition to degenerated myelin in many axons. **(Ae, Af)** In ALS mice treated with high cell-dose, numerous capillaries demonstrated typical endothelium morphology. Normal ultrastructural morphologies of endothelial cells and pericytes, adjacent astrocyte end-feet, and preserved axonal myelin were observed. Only small areas of perivascular edema were seen. En – endothelial cell, Tj – tight junction, BM – basement membrane, P - pericyte, Ast – astrocyte, A – axon, m – mitochondrion, v – vacuole, pl – platelets, Nu – nuclei, * - perivascular edema. Scale bar in a-f is 500 nm. **(B)** *Quantitative analysis of capillary morphology.* Capillary profiles in the lumbar spinal cords were similar to those in the cervical spinal cords. Control mice showed a high percentage of capillaries with normal morphology and a low percentage of moderately impaired capillaries. Media-treated mice demonstrated a significant reduction of morphologically normal capillaries, an increase of capillaries with moderate impairment, and a high percentage of severely damaged microvessels. Steadily increasing percentages of capillaries with normal morphology were determined in cell-treated mice with increased cell dose. A significant increase of normal capillaries was demonstrated in mice receiving the high cell-dose compared to low or mid cell dose treated animals. The percentage of severely compromised capillaries was significantly reduced in mice treated with the high cell dose. The percentages of capillaries with moderate impairment were increased in low or mid cell-treated mice vs. media, whereas a minor percentage decrease was noted in mice receiving the high cell-dose. *$p < 0.05$, **$p < 0.01$.

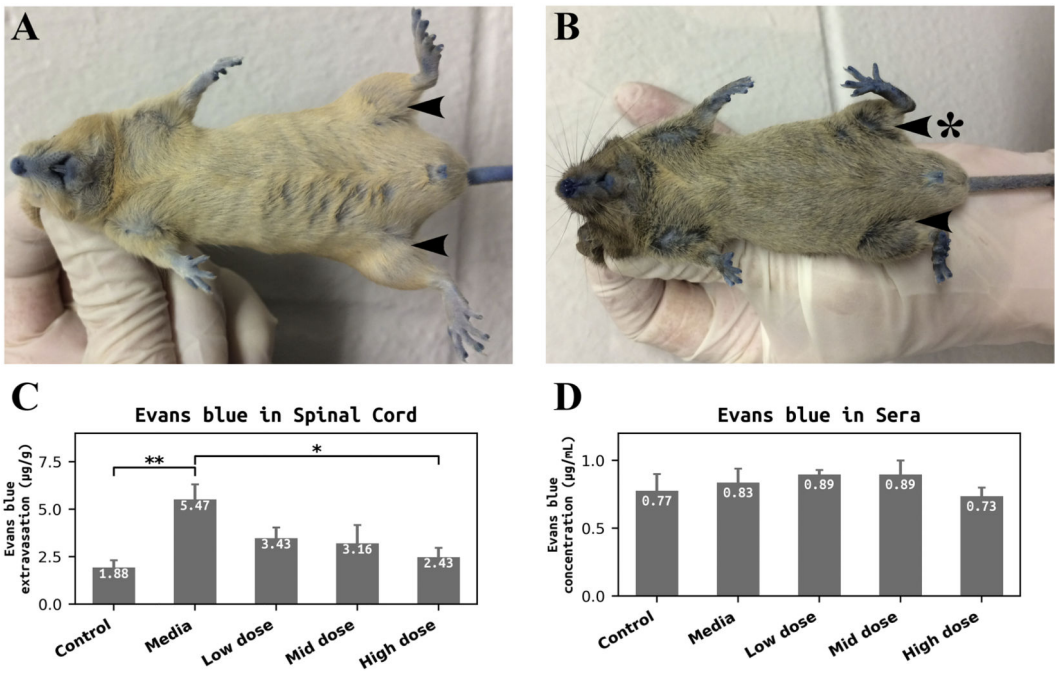


**Figure 3. Quantitative analysis of Evans Blue extravasation into the spinal cord parenchyma of G93A mice and dye concentration in sera.**

Photographs of control **(A)** and media-treated **(B)** mice demonstrated EB penetration (blue color) under skin due to fenestration of capillaries. Visible atrophy in lower posterior, anterior thigh, and medial thigh muscle of media mouse left hindlimb was observed **(B, arrow with asterisk)** compared to normal seeming muscle in hindlimbs of control mouse at the same age **(A, arrows)**. **(C)** Significantly higher levels of EB extravasation were determined in the spinal cords of media-treated mice vs. controls. ALS mice receiving the low or mid dose of hBM34+ cells showed a non-significant decrease of EB levels in tissues vs. media mice. A significant reduction of EB extravasation was found in mice after high cell-dose transplantation. **(D)** There were no significant differences in EB concentration in sera between control, media, and cell-treated mice. *$p < 0.05$, **$p < 0.01$.

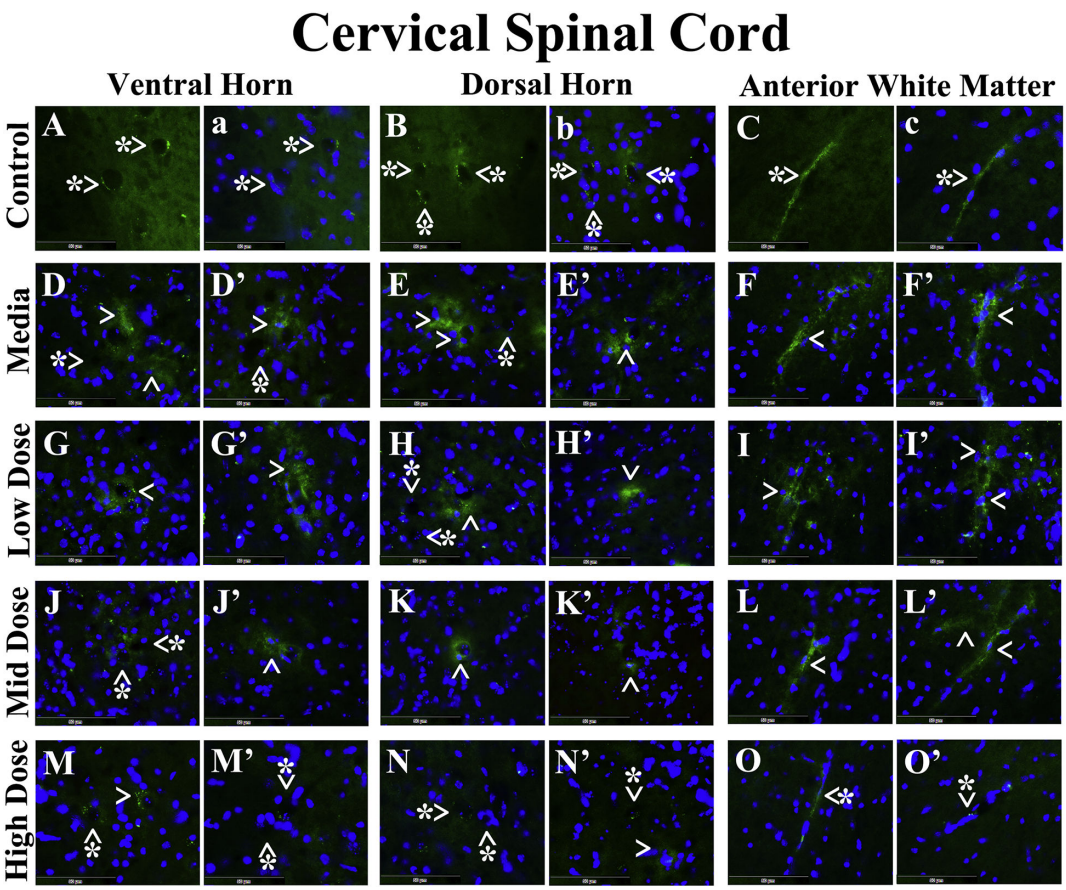


**Figure 4. Evans Blue fluorescence in the cervical spinal cord parenchyma of G93A mice.**

In the cervical spinal cord, EB was clearly detected within the blood vessels (green, arrowheads with asterisks) in the ventral horn **(A, a)**, dorsal horn **(B, b)**, and anterior white matter **(C, c)** from control mice at 17 weeks of age. Vascular leakage (green, arrowheads) of EB, even at some distance from capillaries, was detected in the ventral horn **(D, D')**, dorsal horn **(E, E')**, and anterior white matter **(F, F')** from media-treated animals of the same age. ALS mice receiving the low cell dose showed notable EB leakage (green, arrowheads) in numerous capillaries of the ventral horn **(G, G')**, dorsal horn **(H, H')**, and anterior white matter **(I, I')**. Fewer microvessels permeable for EB (green, arrowheads) were determined in analyzed spinal cord areas **(J-L')** from mice treated with mid cell dose. Considerable reductions of leaky capillaries (green, arrowheads with asterisks) in the ventral horn **(M, M')**, dorsal horn **(N, N')**, and anterior white matter **(O, O')** were detected in ALS mice after receiving the high cell dose. Note, no capillaries leaking EB (arrowheads with asterisks) were observed in the ventral **(D, D')** or dorsal **(E)** horns of media mice or in the dorsal horn of low dose **(H)** or ventral horn of mid dose **(J)** celltreated animals. The nuclei in a, b, c, D-O' are shown with DAPI. Scale bar in A-O' is 50 μm.

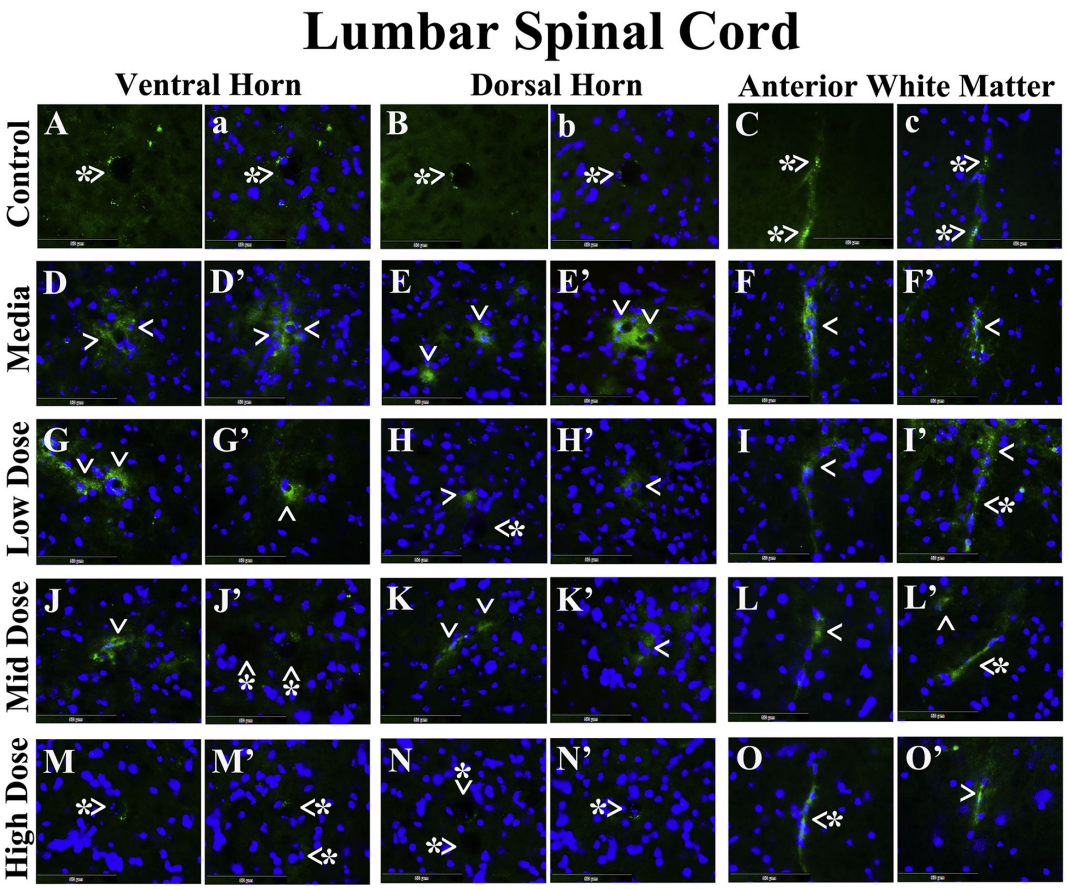


**Figure 5. Evans Blue fluorescence in the lumbar spinal cord parenchyma of G93A mice.**

In the lumbar spinal cord, EB dye was observed intravascularly (green, arrowheads with asterisks) in the ventral horn **(A, a)**, dorsal horn **(B, b)**, and anterior white matter **(C, c)** from control mice, similar to cervical spinal cord results. Significant diffusion of EB (green, arrowheads) into the spinal cord parenchyma from numerous blood vessels was detected in the ventral horn **(D, D')**, dorsal horn **(E, E')**, and anterior white matter **(F, F')** from mediatreated mice. Analogous EB extravasation (green, arrowheads) was seen in analyzed spinal cord areas from mice treated with low **(G-I')** or mid **(J-L')** cell dose. Reduced capillary permeability (green, arrowheads with asterisks) was shown in the ventral horn **(M, M')**, dorsal horn **(N, N')**, and anterior white matter **(O, O')** from the high cell-treated mice. The nuclei in a, b, c, D-O' are shown with DAPI. Scale bar in A-O' is 50 μm.

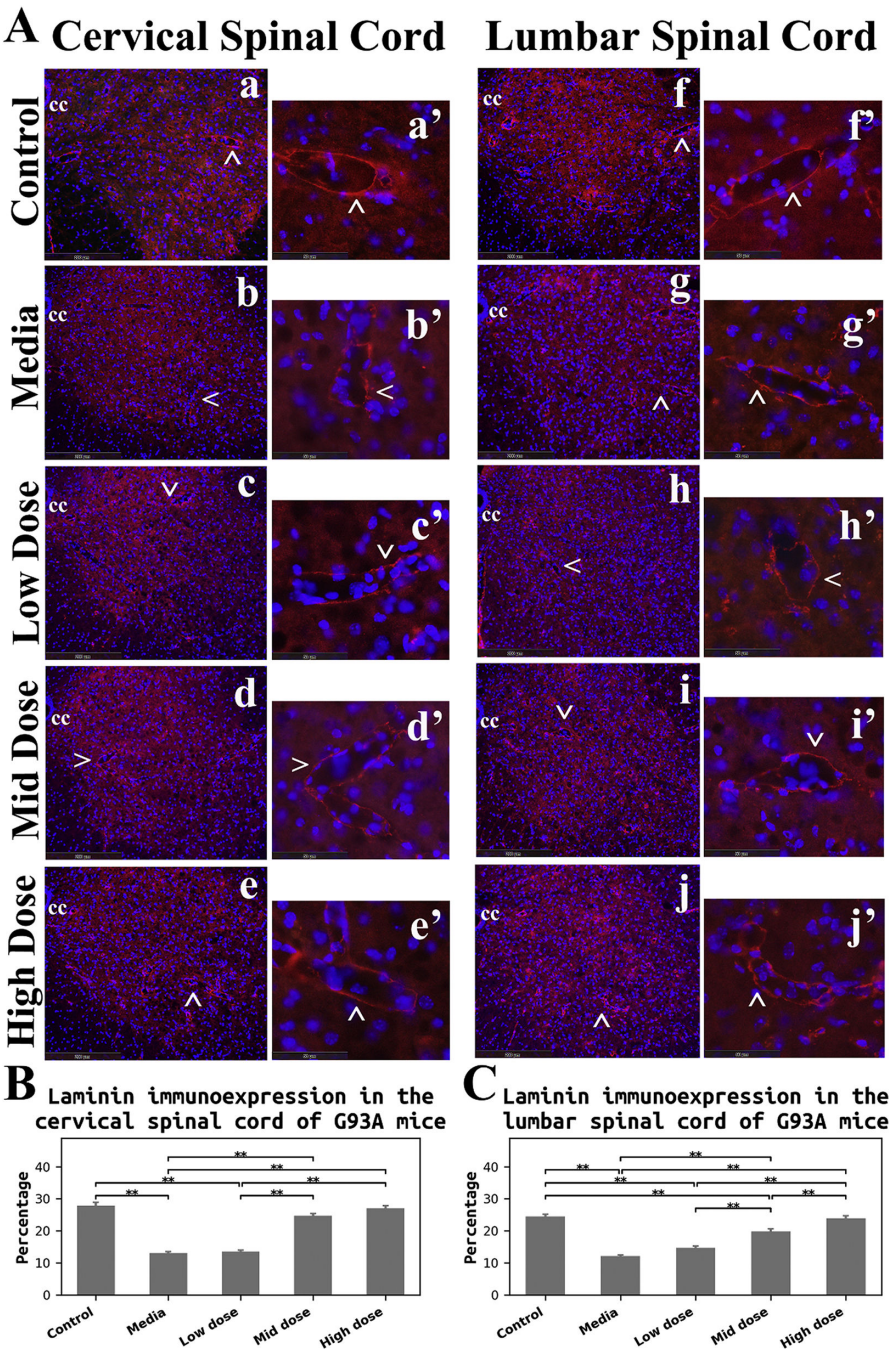


**Figure 6. Immunohistochemical analysis of laminin in the spinal cord of G93A mice.**

**(A)** *Immunofluorescence staining for laminin in the spinal cords.* In control mice, immunostaining for laminin (red) demonstrated well organized microvasculature networks in the cervical **(a)** and lumbar **(f)** ventral horns. Spinal cord capillaries displayed a continuous layer of laminin immunoexpression (red, cervical: **a'**, lumbar: **f'**) in these animals. Substantial reductions of laminin immunoexpression (red) in microvessels were determined in both cervical **(b)** and lumbar **(g)** spinal cords of media-treated ALS mice. Irregularities of laminin staining were obvious in the ventral horn of cervical **(b')** and

lumbar **(g')** spinal cords. ALS mice receiving the low cell dose showed similar patterning of laminin immunoexpression (red) in the spinal cords (cervical: **c, c'**, lumbar: **h, h'**) as in media mice. Increased numbers of capillaries with adequate laminin expression (red) were observed in the cervical and lumbar spinal cords of mice-treated with mid (cervical: **d, d'**, lumbar: **i, i'**) and high (cervical: **e, e'**, lumbar: **j, j'**) cell doses. More robust capillary laminin staining was apparent after the high cell-dose treatment (red, cervical: **e'**, lumbar: **j'**) vs. mid cell-dose. The locations of high magnification images of capillaries in a', b', c', d', e', f', g', h', i', and j' are indicated by arrows in a, b, c, d, e, f, g, h, i, and j. cc – central canal. The nuclei in all images are shown with DAPI. Scale bar in a-j is 200 μm, in a'-j' is 50 μm. **(B)** *Quantitative analysis of laminin immunoexpressions in the cervical ventral horn.* Media-treated mice showed a significant reduction of laminin expression vs. controls. There were no significant differences between the low cell-dose treatment and media mice. Yet, mice receiving the mid and high cell-doses demonstrated significant increases of laminin immunostaining vs. media-treated or low cell-treated animals. **(C)** *Quantitative analysis of laminin immunoexpressions in the lumbar ventral horn.* A *s*ignificant decrease of laminin detection was determined in media mice, similar to findings in the cervical spinal cord. Although no significant differences were found in mice receiving the low cell-dose compared to media, significantly elevated laminin immunostaining was detected in mice treated with the mid and high cell-doses vs. media and low cell-dose. Also, high cell-dose mice showed significantly higher percentage of laminin expression compared to mid cell-dose treated animals. $^{**}p < 0.01$.

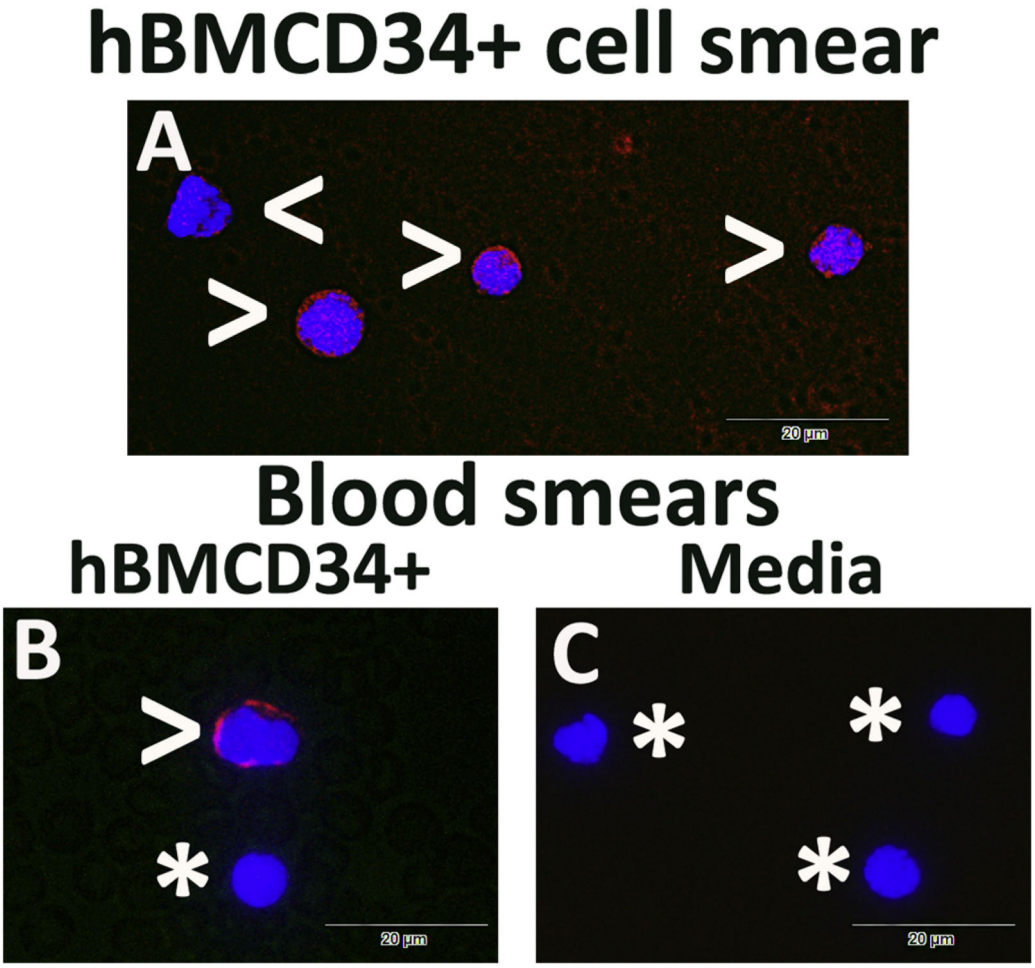


**Figure 7. Immunocytochemical analysis of transplanted hBM34+ cells in blood smears.**

**(A)** All hBM34+ cells were positive for HuNu immunoexpression (red, arrowheads). **(B)** In blood smears from ALS mice receiving the high cell-dose, some cells were identified with the HuNu marker (red, arrowhead). Cells negative for HuNu were noted by asterisks. **(C)** There was no detection of human cells in blood smears from mediatreated mice (asterisks). The nuclei in all images are shown with DAPI. Scale bar in A-C is 20 μm.

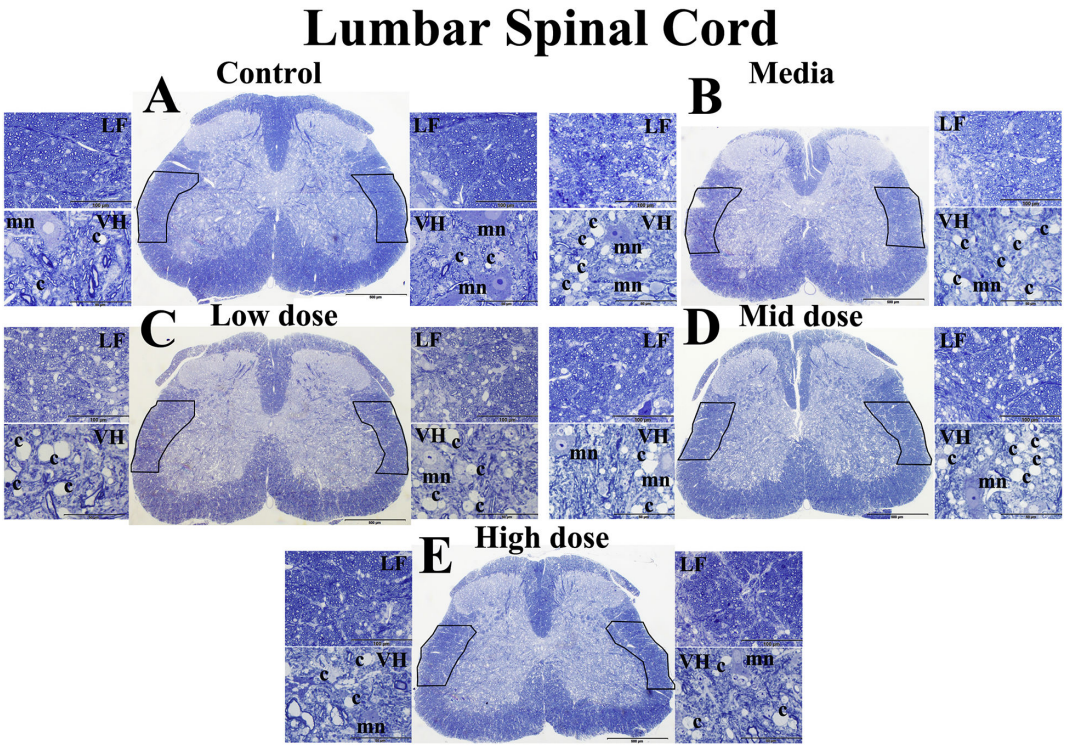


**Figure 8. Histological analysis of myelin and capillaries in the lumbar spinal cord of G93A mice.**

**(A)** Control mice demonstrated well myelinated axons (blue) in lateral funiculus (LF) and ventral horn (VH) of control mice. Typical motor neurons (light blue) and capillaries were observed in VH of these mice. **(B)** Mediatreated ALS mice showed substantially decreased myelin intensity in LF and VH. Motor neurons were reduced in size or degenerated and capillary appearance seemed to increase. Myelinated axons in LF of low **(C)** and mid **(D)** cell-dose treated mice showed moderate increases compared to media mice. Motor neurons in these mice were morphologically adequate. High numbers of capillaries were detected in VH of these cell-treated animals. Dilated capillaries were noted **(C)**. **(E)** ALS mice receiving the high cell-dose showed substantial enhancement of myelin in LF and VH similar to controls. Capillary numbers in VH appeared to decrease. LF – lateral funiculus, VH – ventral horn, mn – motor neuron, c – capillary. Boxes in full spinal cord images delineate LF on both sides. Scale bar in A-E for full spinal cord is 500 μm, for LF is 100 μm, and for VH is 50 μm.

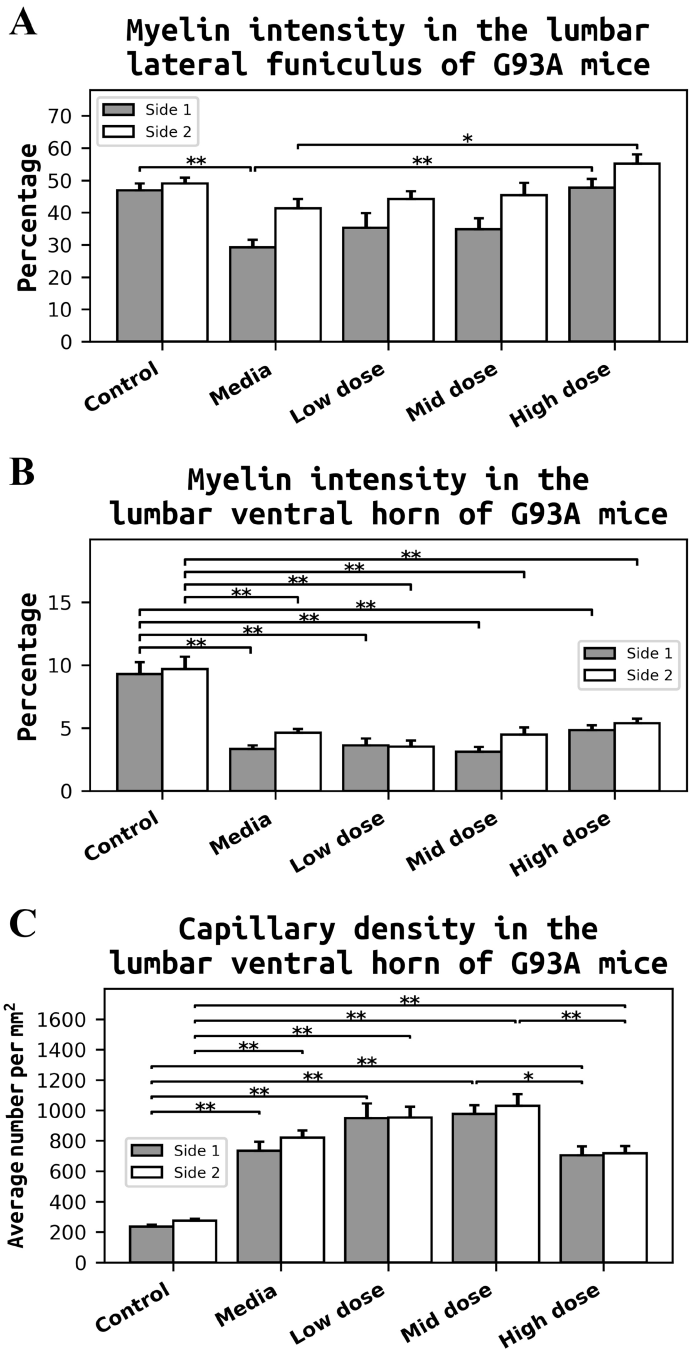


**Figure 9. Quantitative analyses of myelin intensity and capillary density in the lumbar spinal cord of G93A mice.**

**(A)** Media-treated ALS mice showed significant decrease of myelin in LF on side 1 of the lumbar spinal cord compared to control mice. There were no significant differences in myelin expressions in LF between the low or mid cell-dose treated mice vs. media. In contrast, mice treated with the high cell-dose demonstrated a significantly increased percentage of myelinated axons in LF on both sides of the lumbar spinal cord compared to media-treated mice. **(B)** Myelin intensity in VH was similar to LF. Significant decreases of

myelin staining were determined in VH of media mice on both sides vs. controls. Although non-significant differences were found in VH myelin of the low or mid cell-dose treated mice vs. media, a trend towards a percentage increase of myelin expression was noted in mice after the high cell-dose treatment. (C) Quantitative analyses of VH of media-treated animals revealed significantly higher capillary densities on both sides of the lumbar spinal cord vs. controls. Continued elevations of capillary densities were also noted on both sides of VH in low and mid cell-dose treated animals compared to media ALS mice. Yet, a significant decrease of capillary density was determined in mice received the high cell-dose vs. mid cell-dose treated animals. *$p < 0.05$, **$p < 0.01$.